Isotopic Separation and Spectroscopy of Ytterbium-173(3/2) using Laser Cooling

Quinton Dayle McKnight

A senior thesis submitted to the faculty of
Brigham Young University
in partial fulfillment of the requirements for the degree of

Bachelor of Science

Scott Bergeson, Advisor

Department of Physics and Astronomy

Brigham Young University

ABSTRACT

Isotopic Separation and Spectroscopy of Ytterbium-173(3/2) using Laser Cooling

Quinton Dayle McKnight
Department of Physics and Astronomy, BYU
Bachelor of Science

A multi-laser approach is used in which we correct errors in the atomic spectroscopy that seriously compromised previous measurements by another group [Phys. Rev. A 76, 062505 (2007)]. We report precision measurements of the ^{173}Yb $6s6p\ ^1P_1^o(F' = 3/2, 7/2)$ transition frequencies. We use a frequency comb to determine the laser frequency. Our work completes a set of isotope- and hyperfine-shift measurements reported in [1], published by our group. The frequency shift between the $6s6p\ ^1P_1^o(F' = \frac{3}{2}, \frac{7}{2})$ levels is 86.29 ± 0.77 MHz. The uncertainty is dominated by quantum interference effects in the excitation and decay pathways. Appendix A is a summary of notes made on an overheating problem encountered in our laboratory, and a copy of both papers on which I was primary author while completing my undergraduate work included at the end of the thesis.

Keywords: [quantum interference, optical pumping, spectroscopy, optical molasses, laser-induced fluorescence, ytterbium]

ACKNOWLEDGMENTS

This research was supported by Brigham Young University and by grants from the National Science Foundation under Grant No. PHY-1500376 and from the Air Force Office of Scientific Research under Grant No. AFOSR-FA9550-17-1-0302

Thank you Dr. Bergeson, for your patience, your passion, and your brilliance. Sometimes it's just as much the teacher that makes you love a subject as the subject itself, and you helped it to be continually exciting.

Thank you, Chris, my amazing wife, for supporting me, standing by me, and being such a good listener. I love you so dearly.

Thank you, Mom and Dad, for helping me become who I am today, and get where I am now.

Contents

Index **26**

List of Figures

Chapter 1

Introduction

1.1 Motivation

In science, incorrect data can be more detrimental than not having any data in the first place. Being able to trust the validity of scientific journals is integral to that journal's value, justifying why many journals use a peer review system to curate their content. Occasionally, however, mistakes slip through, one such case motivates this research.

The data in question were published by the research group of D. Das and V. Natarajan (DN) in [2], which reports on the transition frequency of the isotopes of ytterbium (Yb). Our own measurements, however, varied widely from those reported by DN. In [1], our research group reports our measurements of all but one of the Yb transition frequencies. In making preliminary measurements of the remaining transition of Yb, we were confident enough in our own measurements to believe that this discrepancy warranted further investigation. We started by double-checking the work of DN to see what they did, and how their methodology differed from our own.

The transition frequency for this difficult to measure transition, the ^{173}Yb $3/2$ hyperfine state, was reported in the work of DN , over three separate papers [2] [3] [4]. DN reported the transition

frequency of the $3/2$ hyperfine state of ^{173}Yb using two separate fitting attempts, confirming said fits by measuring it manually. A recreation of their fitting method is shown in Fig. 1.1(a). The importance of Fig. 1.1(b) will be discussed later in this paper. As is also shown in this thesis, however, there were errors in both their methodology and their data analysis.

1.2 The Importance of Spectroscopy

Mapping the transition spectrum of atoms and their isotopes allows physicists to reliably determine the isotopes in a sample quickly and easily. Atoms always tend toward their lowest energy configuration. Due to aspects unique to each element and isotope, the lowest energy configuration differs, as do the possible excited states. Each little difference in these energy configurations mean that when an isotope is excited by absorbing enough energy, the resulting fluorescence as the atom returns to its ground state has a different wavelength than other transitions, resulting in emission spectra. Similarly, these differences in atomic structure also mean that different isotopes absorb certain wavelengths of light, resulting in the absorption spectra. The frequencies associated with these wavelengths are referred to as atomic transition frequencies, sometimes also known as atomic frequencies or transition frequencies.

By using a photomultiplier tube (PMT) to detect the light fluorescing from an atomic sample we are able to measure the fluoresced light. As we vary the optical frequency of a laser passing through the sample, or scan the laser frequency, we measure which wavelengths of light are absorbed by the isotopes within the atomic sample from the intensity of the fluoresced light. By compiling data points of the measured fluorescence as this fluorescence beam is scanned across a frequency range, we are able to determine the frequencies absorbed by different isotopes. When combined with our knowledge of allowed transitions in each isotope, these fluorescence measurements can tell us which isotopes correspond to each fluorescence peak in the measurement, as well as which

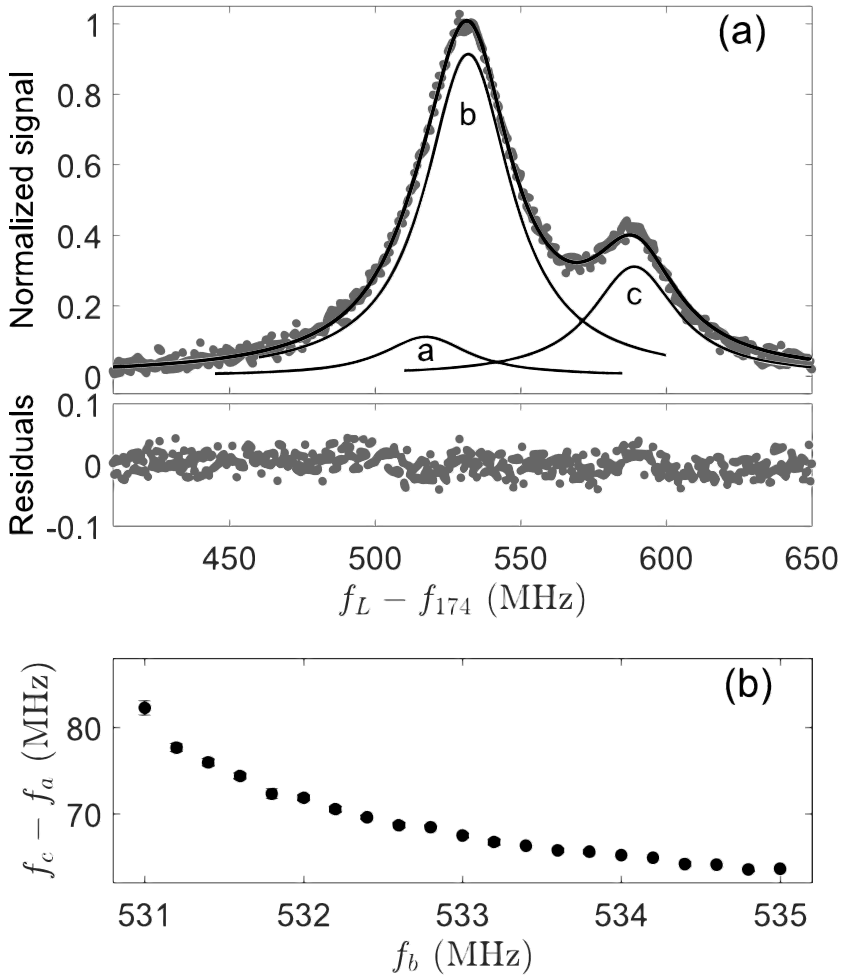

Figure 1.1 The ^{173}Yb-$3/2$ peak extraction reported by DN in their first two papers, recreated by our research group. By applying pseudo-random noise to a computer-generated double peak of ^{172}Yb and the $7/2$ hyperfine state of ^{173}Yb, we are able to demonstrate the fallibility of peak extraction. The problems with this method will be discussed in Section 1.3. (a) The general method used by DN is shown. By fixing the location of the "b" and "c" peaks, the "a" peak can be extracted. The residuals of the pseudo-random noise are shown below the main plot. (b) The extracted location of the "a" peak, shown as a function of variation in the location of the "b" peak. Taken with permission from [5]

hyperfine state (when applicable) occurs in that transition.

This information is valuable in almost any application requiring optical manipulation of atoms. One such application is identifying the proper frequency at which to trap atoms to attain the maximum possible number of atoms trapped, such as when using one of the magneto-optical traps in our laboratory. When the frequency needed to excite specific transitions is not known or is inaccurately known, there can be difficulties in finding and trapping atoms.

Our lab is capable of precision spectroscopy through a number of technological advantages we have over many other spectroscopy labs. One such advantage, known as an optical frequency comb, allows us to lock our lasers to precise frequencies, giving us more reliability in laser frequency measurements. The optical frequency comb, which earned John Hall and Theodore Hänsch half of the Nobel Prize in physics in 2005 [6], makes it possible to measure laser frequencies directly, allowing us to achieve precision of ten significant figures [7]. Our laboratory's previous measurements of the Yb atomic transition frequencies are shown in Fig. 1.2. It is important to note that ^{174}Yb is used as the center point, being the most abundant isotope and therefore the strongest signal. The absolute frequency of ^{174}Yb being

$$f_0 = 751526533.49(33) \tag{1.1}$$

MHz. Because the difference between each isotope and hyperfine state would be six digits into an absolute frequency measurement, it is easier to show these differences as relative to the ^{174}Yb absolute measurement

1.3 Difficulties In Identifying Peaks

Often, identifying specific peaks from fluorescence scan data can be done quite reliably, but in the case of Yb, there are some complications around the lines of ^{172}Yb and the $3/2$ and $7/2$ hyperfine states of ^{173}Yb. In Fig. 1.2 it can be seen that the $3/2$ hyperfine state of ^{173}Yb is blended with the

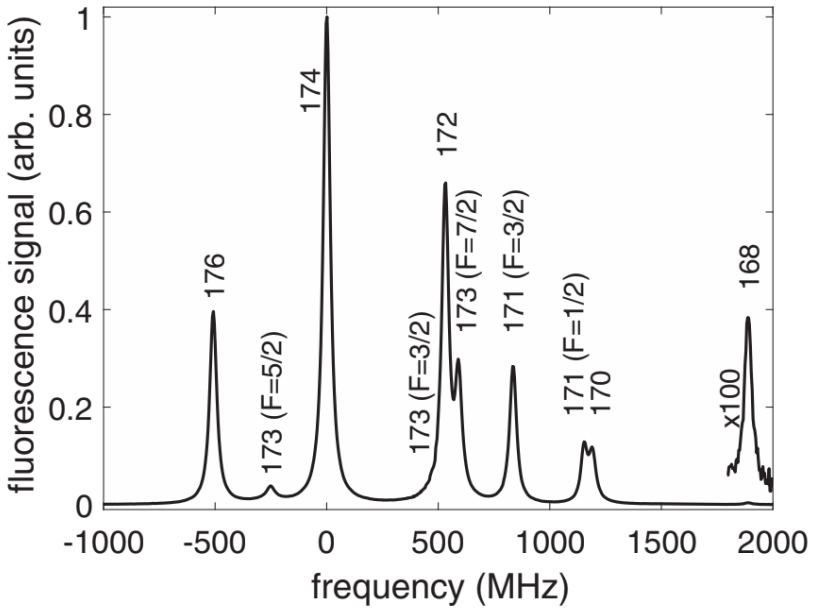

Figure 1.2 The different isotopes and hyperfine states of ytterbium as they appear according to frequency of light used to scan. Taken with permission from [1]

peak of ^{172}Yb, such that the $3/2$ hyperfine state cannot be differentiated. In the first two papers produced by DN on this subject, they used measurements of the transition frequency of ^{172}Yb and the $3/2$ and $7/2$ hyperfine states of ^{173}Yb for their data analysis. As shown in Fig. 1.1(a), By fixing the frequencies of the "b" and "c" peaks in their fit, they are able to use a fitting algorithm to find the location of the $3/2$ hyperfine state at "a". This methodology can be called into question. If the frequency of the "b" peak is varied, the difference between the "a" and "c" peak can vary greatly, as is shown in Fig. 1.2(b). This shows the necessity of a more direct measurement of the $3/2$ hyperfine state using isotopic purification, and that these peak locations cannot be extracted through simple peak fitting procedures. The process of isotopic purification is discussed in more detail in chapter 2.

1.4 Optical Pumping Problem

An additional spectroscopic consideration is related to the third paper published by DN on this specific measurement related to something called optical pumping. Optical pumping is an effect that occurs when the lower level of a transition has more available sub-levels than the upper level. The fluorescence beam exciting the atoms determines the change in the magnetic quantum number, Δm: $\Delta m = 0$ for linearly polarized light, $\Delta m = 1$ for right-hand circularly polarized light, and $\Delta m = -1$ for left-hand circularly polarized light. This in itself wouldn't be a problem, but when the atoms decay back down to the ground state, $\Delta m = 0, \pm 1$, regardless of the excitation Δm.

In the specific case of the upper state of ^{173}Yb, for linearly polarized light, any of the atoms that go into the $\pm 5/2$ sub-levels of the lower state will no longer be excited to the $3/2$ hyperfine state. This unavailability is known as optical pumping. The optical pumping of ^{173}Yb is shown in Fig. 1.4, where the atoms are always within two transitions of being unreachable. The probability of atoms in the upper state going to any given lower state is determined by the Clebsch-Gordan coefficients. The probabilities for ^{173}Yb are given in [8]. In our experiment, we found that the ^{173}Yb atoms were unable to reach the $3/2$ hyperfine state after approximately one microsecond of exposure to the fluorescence beam at the $3/2$ frequency, even though the atoms traveled through the beam in $20 - 30$ microseconds, depending on the velocity of the atoms. The atoms were effectively "blind" to the laser, and therefore did not give off the fluorescence we needed to measure for a majority of the time they were exposed to the laser. This problem can be solved by introducing a repumper beam, which pumps the trapped atoms to the $5/2$ hyperfine state, allowing them to decay back to sub-levels accessible to the $3/2$ beam.

Nowhere in the paper by DN is a repumper beam mentioned or shown, leading us to assume they did not use one. These physical limitations when a repumper is not used calls into question how they would be able to see the $3/2$ hyperfine state at all. Our data, which illustrates the need of a repumper beam, can be seen in Fig. 3.1.

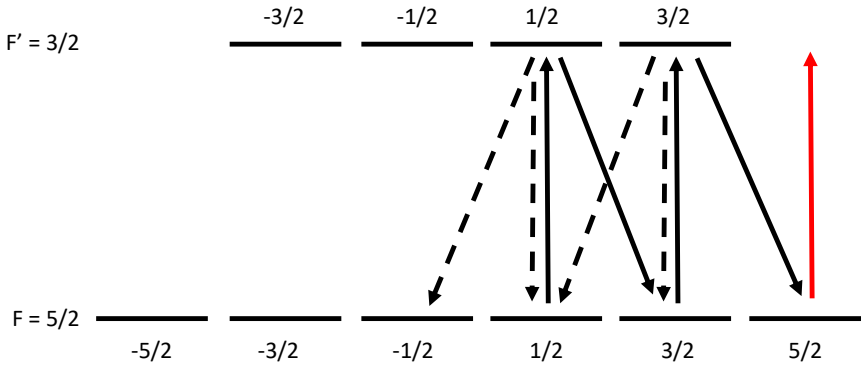

Figure 1.3 This figure shows the ground state and the $3/2$ hyperfine state of ^{173}Yb, depicting how atoms can stop being able to communicate with the beam used to excite the atoms to the $3/2$ hyperfine state. The solid arrows show the path hypothetically taken, while the dotted arrows show the other possible decay paths. The red arrow shows that lower state atoms in $\Delta m = \pm 5/2$ can no longer be excited to the upper state.

1.5 Quantum Interference

Another consideration necessary in spectroscopy is known as quantum interference. Quantum interference occurs due to multiple quantum pathways being available for the atom to get from one state to another. Atomic transition frequencies can accurately be modeled as Lorentzian line shapes. Because of this line shape, atomic transitions can happen near a transition frequency, and not exclusively at the exact frequency of the peak. Therefore a non-zero probability of atoms using different atomic transitions to arrive at the same end state exists, even when using a frequency at or near a specific transition. Multiple available pathways can result in a shift of the perceived location of the atomic frequency. When the fluorescence beam's polarization and the angle of the scattered light relative to the PMT are at a "magic angle," this effect is eliminated, giving us the true transition frequency [9].

1.6 Overview

Our measurements, using multiple frequency comb-locked lasers, disagree with DN's measurements, and we report mistakes made in DN's methodology. Though DN 's reported precision is better, the fact that they didn’t correct the optical pumping problem means this measurement should not be possible in the first place, and disregarding quantum interference would add 3 MHz uncertainty on its own.

Chapter 2

Methods

2.1 DN's Design

The design used by DN, as depicted in Fig 2 of [2], uses a Yb source, heated to sublimation, creating an atomic beam [2]. That atomic beam goes through a one dimensional optical molasses, discussed in Section 2.3, which deflects the ^{173}Yb isotope into a side channel, isotopically separating it from the rest of the Yb. This allows the measurement of ^{173}Yb free from ^{172}Yb. By performing spectroscopy on both the main arm and the side arm, the amount of ^{173}Yb in both can also be measured, as DN reports in Fig 3(c) of [2]. What is concerning is that the deflection percentage reported by DN should not be possible based on their laser power, their experimental design, and our findings. The atomic velocities of the sublimated atomic beam are too high to be fully captured by the optical molasses. As such, the deflection percentage reported by DN is called into question.

This design, while in principle effective, uses one laser and a number of acousto-optical modulators (AOMs), which could be replaced by using multiple lasers. As we have the lasers necessary, we forego the AOMs in place of multiple separate lasers, providing numerous advantages. Our lasers are locked to an optical frequency comb. However, by using multiple lasers, we are able

to freely sweep the frequency of any individual laser while the other lasers stay at their original frequency. The DN system does not allow for this. This difference allows us greater freedom in our measurements.

2.2 Our Design

Our final design uses an experimental setup similar to that used by DN in their experiment, with the addition of a repumper laser and the advantages of multiple lasers locked to an optical frequency comb, as mentioned above. The repumper beam pumps the atoms into the $5/2$ hyperfine state, allowing an equalization of the ground state magnetic sublevels. The interaction of the repumper beam and the magnetic sublevels is shown in Fig. 2.1, where the optical pumping into an unavailable magnetic sublevel and the repumping into available sublevels is shown through the black and blue lines respectively. The addition of an optical frequency comb into our system allowed us an advantage on frequency precision. Using this method, the error within our laser frequency is reduced to 40 kHz ($\mathrm{d}f/\mathrm{d} = 1 * 10^{-10}$). As shown in Fig. 2.2, as the atomic beam progresses along the channel, ^{173}Yb is deflected through the upper channel. Once the isotopically pure ^{173}Yb reaches the end of the tunnel, the repumper makes it possible for the probe beam to incite fluorescence in the individual hyperfine states of ^{173}Yb.

By measuring the fluorescence from the side arm, we can determine which hyperfine states are present. This is where the repumper beam becomes necessary, because without it, there will be no $3/2$ hyperfine state present in the side arm due to optical pumping. Based on the polarization of the light used in fluorescence, the ground state ^{173}Yb is sent into different magnetic sub-levels. Without a repumper beam, optical pumping would mean that before we could even register the presence of the $3/2$ hyperfine state in our measurements, it would already be impossible to send atoms into said state.

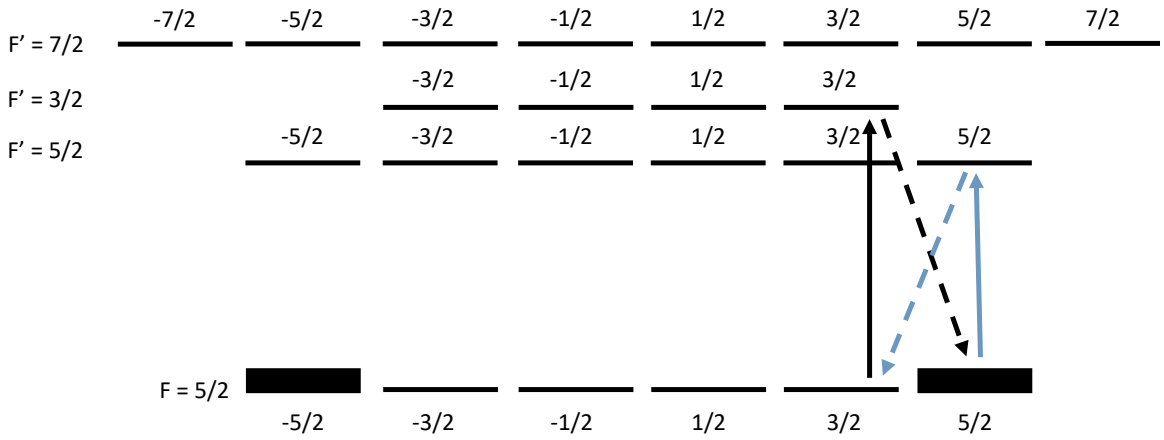

Figure 2.1 Optical pumping causes all the atoms being excited into the $3/2$ hyperfine state to end up in the $m = \pm 5/2$ sublevels. Sublevel populations are shown by the thickness of ground state sublevel lines. When a repumper beam is applied, the sublevel populations can be redistributed. The black arrows represent optical pumping into the $\pm 5/2$ sublevels, while the blue arrows represent the repumper beam returning the atoms to sublevels reachable by the fluorescence beam.

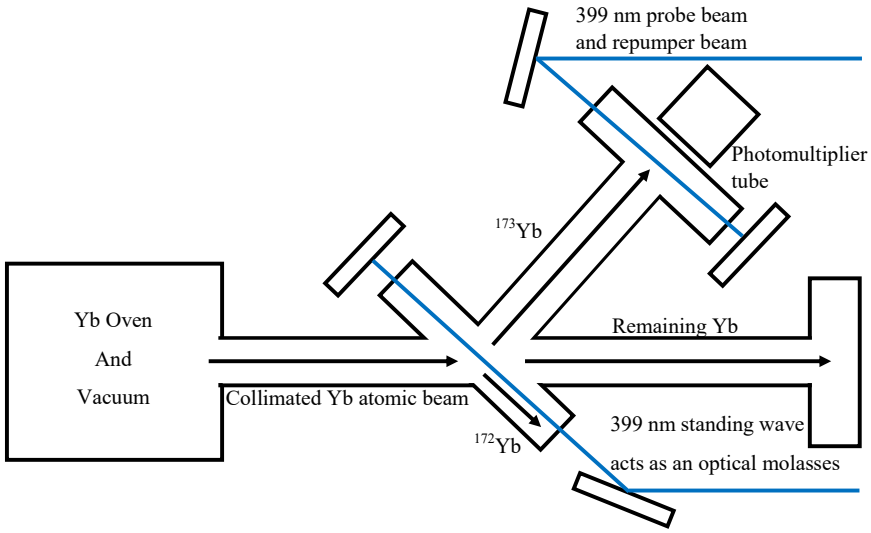

Figure 2.2 Sublimated Yb travels from the left to the right as an atomic beam. While ^{173}Yb is deflected into the upper channel because of the 399 nm standing wave, ^{172}Yb is deflected the other direction. This results in the upper channel having an isotopically pure beam of ^{173}Yb.

2.3 One Dimensional Optical Molasses

By using a retroreflected laser to create a standing wave, we can redirect selected isotopes of atoms by detuning the laser to act as a one dimensional optical molasses. A one dimensional optical molasses slows atoms in the direction of the standing wave. The velocity of atoms can be changed by absorbing momentum from the photons. This only occurs, however, if the photons are of the right wavelength to be absorbed by the atoms. The correct wavelength changes relative to the atomic velocity in the direction of the light source due to Doppler shifting. This all means that a one dimensional optical molasses only influences atoms moving at a specific range of velocities, catching only a fraction of the atoms in the atomic beam. Because each isotope is influenced by a different wavelength of light, by carefully selecting our wavelength, adjusting for the velocity-induced Doppler shift, we are able to slow the ^{173}Yb in the direction perpendicular to our chamber's side arm, resulting in the atoms changing direction into the side arm. In our experiment, we slowed the $7/2$ hyperfine state of ^{173}Yb.

The choice of deflection angle is important in this experiment because the smaller the angle, the more atoms you will capture. If the angle is too small, however, the atoms in the side arm are not isotopically pure. Keeping the side arm isotopically pure is important, because ^{172}Yb is sufficiently abundant and its transition frequency is close enough to ^{173}Yb in the 3/2 hyperfine state that frequency measurements become unreliable if there is any ^{172}Yb present.

The velocity distribution of the atoms is described by

$$f(v) \approx v^3 e^{\frac{-mv^2}{2k_B T}}, \tag{2.1}$$

where v is the velocity of the atoms, m is the mass of Yb, k_B is the Boltzmann constant and T is the temperature of the atoms. Our atoms are heated to 500 °C. By choosing a detuning $-\Delta$, measured in MHz, and the angle of the optical molasses measured perpendicular to the atomic beam, we can calculate the percentage of atoms captured. The equation for the atomic

Doppler shift, $\frac{1}{\lambda} v sin(\theta) = \Delta$, with some rearranging, provides us with the optimal velocity of atoms deflected by the molasses, $v_d = \frac{\lambda \Delta}{sin(\theta)}$. $v_{max} = v_d + v_N$ is the maximum velocity deflected, where $v_c = \lambda \nu_N = (399nm)(28MHz) = 11.172m/s$ is the centerline of the capture velocity. ν_N in this equation is the natural linewidth. Likewise, v_{min}, the minimum velocity captured, is $v_d - v_N$ when positive, or 0. In the regime used here v_{min} is always zero. All of this allows us to find the ratio of atoms deflected,

$$R_d = \frac{\int_{v_{min}}^{v_{max}} v^3 e^{\frac{-mv^2}{2k_B T}} dv}{\int_0^{\infty} v^3 e^{\frac{-mv^2}{2k_B T}} dv}. \tag{2.2}$$

We used a detuning of 40 MHz in our experiment, with our lasers locked to 399 nm. Using this detuning, we are able to capture atoms up to $33.74m/s$ using a deflection angle of 45°, which comprises 0.12% of the atoms in the atomic beam. While reducing our deflection angle to 38°would double our signal, we obtain a strong enough signal from 45°to make a valid measurement.

The angle from which you observe the atoms is also important, because fluorescence of some isotopes is angle dependent, so observations from other angles do not see anything. This is well documented in [10], where it is shown that many of the isotopes and hyperfine states of Yb can be seen most easily when observed from a direction perpendicular to both the atomic beam and the fluorescence beam. This effect is less prevalent in the hyperfine states of ^{173}Yb, though they are still present for some hyperfine states. It seems possible to measure ^{173}Yb in the $3/2$ hyperfine state even while ^{172}Yb is present by taking advantage of this, but even though computational models report that visibility of ^{172}Yb should reach zero, in our experimental design this is not feasible. Because both our light source and our PMT are not point sources, we collect enough light outside of the solid angle where ^{172}Yb has no visibility that this is still a problem. The result is that isotopic separation is still the most viable method in the end.

Chapter 3

Results

3.1 Data

All numerical reports of hyperfine transitions in our data are given relative to the absolute transition frequency, f_0, our research group has measured for ^{174}Yb. This measurement of $f_0 =$ 751526533.490.33 MHz, reported in [1], is used as the "zero" in our other measurements. Our reported measurements of the Yb-173 $6s^2\ ^1S_0 - 6s6p\ ^1P_1^o\ (F' = 3/2)$ and $(F' = 7/2)$ transition frequencies, relative to ^{174}Yb, are

$$\begin{aligned} 6s^2\ ^1S_0 - 6s6p\ ^1P_1^o\ (F' = 3/2) \quad 503.22 \pm 0.70 \text{ MHz} \\ 6s^2\ ^1S_0 - 6s6p\ ^1P_1^o\ (F' = 7/2) \quad 589.51 \pm 0.33 \text{ MHz}. \end{aligned} \tag{3.1}$$

The difference measured between these two hyperfine states is 83.7 ± 0.77 MHz. Our data is shown in Fig. 3.1, where Fig. 3.1(a) shows the isotopically pure ^{173}Yb, and Fig. 3.1(b) shows both ^{173}Yb and ^{172}Yb. Additionally, both Fig. 3.1(a) and Fig. 3.1(b) show what is measured with a repumper beam, in blue, and without, in black. When taking these factors into account, it is clear both that isotopic purification is necessary in these measurements, and that without a repumper beam the ^{173}Yb $3/2$ hyperfine transition is impossible to measure with this configuration.

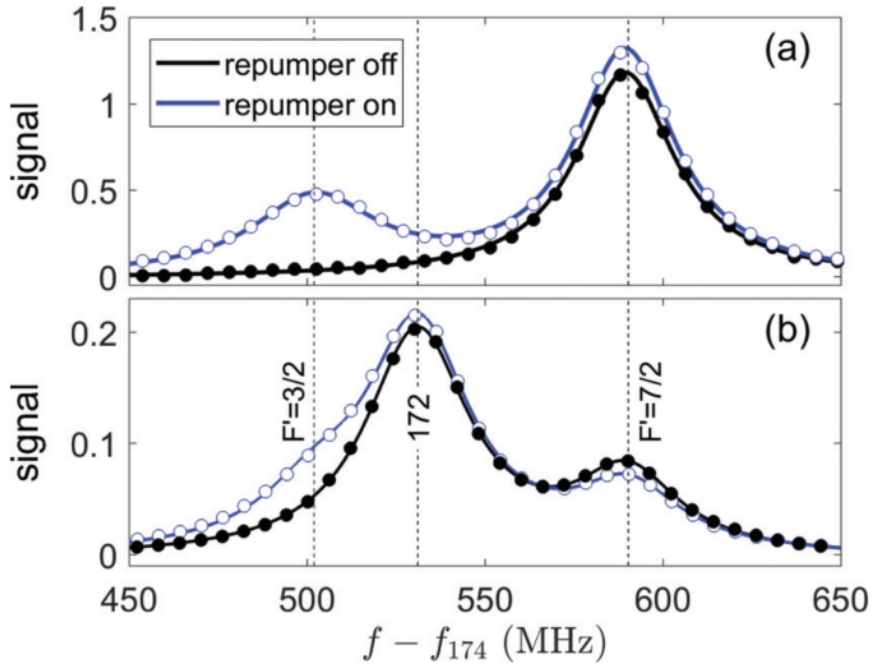

Figure 3.1 This figure illustrates the difference between scanning with the fluorescence laser with and without a repumper beam. As can be seen in (a), in the presence of a repumper beam the $F' = 3/2$ peak is clearly visible, while without the repumper it is not visible. In (b) the importance of isotopic purification in measuring $F' = 3/2$ is clearly shown. Taken with permission from [5]

3.2 Analysis of Data

These transition frequencies are not easily compared to the measurements reported by other groups because instead of reporting frequency most other groups report using the hyperfine constants of the Hamiltonian originally introduced in [11]. This Hamiltonian is

$$W_F = \frac{1}{2}hAK + hB\frac{\frac{3}{2}K(K+1) - 2I(I+1)J(J+1)}{2I(2I-1)2J(2J-1)} \tag{3.2}$$

, where $K = F(F+1) - I(I+1) - J(J+1)$. This gives a solution that can be used to solve for the hyperfine constants A and B using our experimental measurements.

In Table 3.1, our measurements are compared to that of other groups using these hyperfine constants. Papers [2], [4], and [3] are the three published by DN and their research group, with the [2] and [4] especially having unrealistically low reported error based on the problems in their methodology mentioned prior. Additionally, [12] uses the same measurement techniques as DN, resulting in similar errors in their measurements.

3.3 Error Analysis

We can attribute errors in our data to two primary categories, those errors pertaining to atomic spectroscopy and those pertaining to laser metrology. Of those two, the errors related to atomic spectroscopy dominate, with one of the primary sources of error in that category being quantum interference. As for laser metrology errors, one of our research group's previous papers [1] carefully categorizes statistical errors, frequency comb errors and cell shift errors.

As discussed in Section 1, the quantum interference errors are quite complicated. Failing dealing with them properly would add an error of ± 3 MHz to our results. Because we aligned our system so that the scattering angle would be $\theta_s = 0$, the fluorescence beam polarization, or "magic angle", that would eliminate quantum interference is $\theta_p = 53.7°$. The graph shown in Fig. 3.2 shows our

measurements of the quantum interference as the polarization beam angle is varied. As the angle is changed from the mathematically correct "magic angle" the perceived transition frequency also changes.

The errors related to laser metrology, all combined, result in the uncertainty of 40 kHz attributed earlier to the optical frequency comb.

3.4 Conclusion

We are confident in our measurements and have found sufficient evidence to conclude that our measurements of the $6s^2\ {}^1S_0(F=\frac{5}{2}) - 6s6p\ {}^1P_1^o(F'=\frac{3}{2},\frac{7}{2})$ transition frequencies in ^{173}Yb are the most reliable currently available. The numbers reported by DN are incorrect, and the error

Table 3.1 Our measurements as compared to similar measurements of the same atomic transition. The year of each paper's publishing is shown in column 2, while columns 3 and 4 show the values measured for the hyperfine constants. Taken with permission from [5]

Method	year	A_{173} (MHz)	B_{173} (MHz)
Our measurements [5]	2017	59.52 ± 0.20	601.87 ± 0.49
beam [12]	2010	57.9 ± 0.2	608.4 ± 0.8
molasses [2]	2007	57.693 ± 0.006	609.028 ± 0.056
beam [4]	2005	57.682 ± 0.029	609.065 ± 0.098
beam [3]	2003	57.91 ± 0.12	610.47 ± 0.84
beam [13]	2002	57.7 ± 0.9	602.1 ± 1.1
level crossing [14]	1985	58.1 ± 0.3	588 ± 2
level crossing [15]	1976	58.45 ± 0.80	589.6 ± 13.0
level crossing [16]	1969	56.9 ± 0.50	575 ± 7

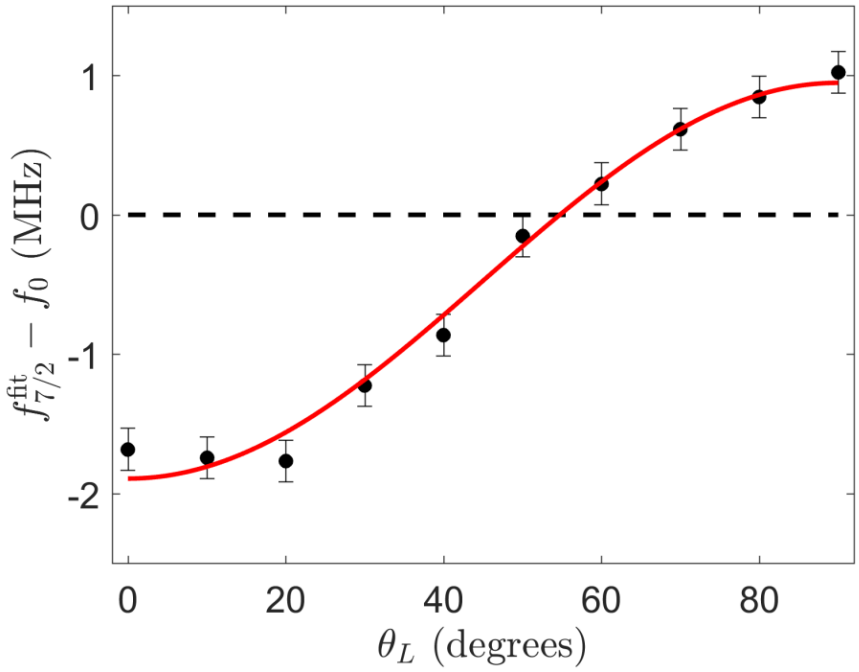

Figure 3.2 Due to many possible pathways in atomic transitions and the broad nature of transition peaks, the perceived frequency of transition peaks can shift based on the viewing angle relative to the angle of fluoresence beam polarization. This effect is eliminated at a polarization of 53.7°. Taken with permission from [8]

bounds are not to be believed. DN did not correctly account for optical pumping and quantum interference, among other effects, resulting in their reported values being unreliable. Our accounting for these effects, and the added precision available due to advantages in our laser system make our measurements more reliable.

Appendix A

Laboratory Thermal Issues Notes and Publications

A.1 Summary

This section is to sum up my efforts over the last few months in the lab, in case the lab starts overheating again in the future. This can be a major issue because thermal variation in the lab causes the laser locks to become unstable. I have worked with John Ellsworth and Dr. Bergeson to test a number of solutions, and at the time of me writing this the problem seems to be solved. Nonetheless, it is always worth keeping notes in case problems need to be revisited.

The first step we took to solve the thermal issues is to contact Facility Management, having them increase the air flow in the lab. They also adjusted the air-flow louvers, working to optimize the cooling in the front of the lab (closer to the entrance doors) more than the back, because a majority of our laser locks are in the front and the major heat sources are in the back. While waiting for Facilities to come, I also removed the vent covers throughout the lab to allow for better conductance.

The second step in solving this problem is identifying that a large amount of the heat in the

lab is due to the pulse lasers and the dye laser pumps. All of these are currently under the back two optics tables in the lab. Prior to dealing with this problem we had a wooden sound-damping enclosure around one of the tables, but we had the machine shop make an enclosure for the other table as well. These enclosures are open toward the back of the lab, ensuring that the heat has a chance to be vented out from the back of the room before it makes its way forward.

The third step, which we have researched but deemed currently unnecessary, is to install air-to-water heat exchangers under each of the wooden enclosures, to get rid of as much heat coming from those tables as possible through water which then gets pumped out of the room. At the time of writing this John Ellsworth is currently working to see about getting colder water pumped to our lab to be used with these heat exchangers.

A.2 Heat Exchangers

The heat exchanger we settled on as being the best for our needs is the ChillX Zephaire 12.5k-50k BTU Modine Style Air-To-Water Heat Exchanger, currently found at this URL: http://chillxchillers.com/air-to-water-heat-exchangers/zephaire-high-speed-air-to-water-heat-exchangers?sku=ZAU0120500ZA-B . While we debated on a number of heat exchangers, this one seemed to be the simplest to implement, the most effective overall, and the cheapest. All in all, a win. All we would have to do to make these heat exchangers work is to install a water line to them from the chilled water supply, and put one exchanger under each of the back tables, inside the wooden enclosures. It could be helpful to try attaching the heat exchanger directly to the pulse laser power supplies, since that is where a majority of the heat is produced.

In the end, I calculated that when all heat sources under each of the back tables are accounted for, the total heat per table, as a high estimate, is less than 2000 W. A majority of this, as mentioned above, is produced by the Surelite III-10 power supplies, which draw 5.5 A at 208 V. Due to the

nature of how lasers work, a majority of this energy is released as heat, resulting in nearly 1200 W of power from each power supply. I honestly hope this problem never resurfaces, but if it does, hopefully these notes can be of use.

A.3 Publications

Included here are the two publications published in our lab in which I was primary author.

Bibliography

[1] M. Kleinert, M. E. Gold Dahl, and S. Bergeson, "Measurement of the Yb I $^1S_0 - ^1P_1$ transition frequency at 399 nm using an optical frequency comb," Phys. Rev. A **94,** 052511 (2016).

[2] D. Das and V. Natarajan, "Laser cooling of ^{173}Yb for isotope separation and precision hyperfine spectroscopy," Phys. Rev. A **76,** 062505 (2007).

[3] A. Banerjee, U. D. Rapol, D. Das, A. Krishna, and V. Natarajan, "Precise measurements of UV atomic lines: Hyperfine structure and isotope shifts in the 398.8 nm line of Yb," EPL (Europhysics Letters) **63,** 340 (2003).

[4] D. Das, S. Barthwal, A. Banerjee, and V. Natarajan, "Absolute frequency measurements in Yb with 0.08 ppb uncertainty: Isotope shifts and hyperfine structure in the 399−nm $^1S_0 \rightarrow ^1 P_1$ line," Phys. Rev. A **72,** 032506 (2005).

[5] Q. McKnight, A. Dodson, T. Sprenkle, T. Bennett, and S. Bergeson, "Comment on "Laser cooling of ^{173}Yb for isotope separation and precision hyperfine spectroscopy"," Phys. Rev. A **97,** 016501 (2018).

[6] Nobelprize.org, "The Nobel Prize in Physics 2005," https://www.nobelprize.org/prizes/physics/2005/summary/ (Accessed February 4, 2019).

[7] M. Lyon and S. D. Bergeson, "Precision spectroscopy using a partially stabilized frequency comb," Appl. Opt. **53,** 5163–5168 (2014).

[8] A. Dodson, "Quantum Interference in the Hyperfine Transitions of Ytterbium,", 2018.

[9] R. C. Brown, S. Wu, J. V. Porto, C. J. Sansonetti, C. E. Simien, S. M. Brewer, J. N. Tan, and J. D. Gillaspy, "Quantum interference and light polarization effects in unresolvable atomic lines: Application to a precise measurement of the ^{6,7}Li D_2 lines," Phys. Rev. A **87,** 032504 (2013).

[10] R. Zinkstok, E. J. van Duijn, S. Witte, and W. Hogervorst, "Hyperfine structure and isotope shift of transitions in Yb I using UV and deep-UV cw laser light and the angular distribution of fluorescence radiation," Journal of Physics B: Atomic, Molecular and Optical Physics **35,** 2693–2701 (2002).

[11] E. Arimondo, M. Inguscio, and P. Violino, "Experimental determinations of the hyperfine structure in the alkali atoms," Rev. Mod. Phys. **49,** 31–75 (1977).

[12] W. Wen-Li and X. Xin-Ye, "A novel method to measure the isotope shifts and hyperfine splittings of all ytterbium isotopes for a 399-nm transition," Chinese Physics B **19,** 123202 (2010).

[13] R. Zinkstok, E. J. van Duijn, S. Witte, and W. Hogervorst, "Hyperfine structure and isotope shift of transitions in Yb I using UV and deep-UV cw laser light and the angular distribution of fluorescence radiation," Journal of Physics B: Atomic, Molecular and Optical Physics **35,** 2693 (2002).

[14] H. Liening, "Level-crossing-spectroscopy with additional optical pumping in the ground state," Zeitschrift für Physik A Atoms and Nuclei **320,** 363–368 (1985).

[15] M. Baumann, H. Liening, and H. Lindel, "Investigation of the HFS in the 6s6p1P1 state of 173Yb(I) LC and AC spectroscopy," Physics Letters A **59,** 433 – 434 (1977).

[16] B. Budick and J. Snir, "Hyperfine Structure of the $6s6p^1P_1$ Level of the Stable Ytterbium Isotopes," Phys. Rev. **178,** 18–23 (1969).

Index

Comment on "Laser cooling of ^{173}Yb for isotope separation and precision hyperfine spectroscopy"

Quinton McKnight, Adam Dodson, Tucker Sprenkle, Tyler Bennett, and Scott Bergeson*
Department of Physics and Astronomy, Brigham Young University, Provo, Utah 84602, USA

(Received 28 September 2017; published 16 January 2018)

We present measurements of the hyperfine splitting in the ^{173}Yb $6s6p\ ^1P^o_1(F' = 3/2,7/2)$ states that disagree significantly with those measured previously by Das and Natarajan [Phys. Rev. A **76**, 062505 (2007)]. We point out inconsistencies in their measurements and suggest that their error is due to optical pumping and improper determination of the atomic line center. Our measurements are made using an optical frequency comb. We use an optical pumping scheme to improve the signal-to-background ratio for the $F' = 3/2$ component.

DOI: 10.1103/PhysRevA.97.016501

I. INTRODUCTION

Measurements of isotope shifts are important for benchmarking atomic structure calculations [1]. They can help address questions of nucleosynthesis in the early universe [2], parity nonconservation [3–5], measuring the charge distribution in the nucleus [6], and constraining the search for new physics beyond the standard model [7]. It is critically important, therefore, that the quality of isotope shift measurements is verified and that systematic errors are properly identified and controlled. In the case of Yb, calculations can be extremely difficult because of significant configuration interaction in the complicated level structure [8].

Ten years ago, Das and Natarajan (DN) published what appeared to be definitive measurements of the hyperfine splitting in the ^{173}Yb $6s6p\ ^1P^o_1(F' = 3/2)$ and $(F' = 7/2)$ levels [9]. They used laser spectroscopy on the $6s^2\ ^1S_0 - 6s6p\ ^1P^o_1$ transition at 399 nm. In a standard laser-induced fluorescence experiment using an atomic beam, these measurements are challenging because the transition in ^{173}Yb to the $(F' = 3/2)$ level is nearly coincident with the resonance transition in ^{172}Yb. To overcome this problem, DN used a one-dimensional optical molasses to selectively deflect ^{173}Yb atoms into a spatially separated slow atomic beam. They performed standard laser-induced fluorescence spectroscopy on the now clearly resolved ^{173}Yb transitions. They reported a frequency splitting of 72.093 ± 0.036 MHz between the $F' = 3/2$ and $F' = 7/2$ levels. This is an excellent method that appears to be plagued by spectroscopy and metrology errors. We have repeated their experiment and measure a frequency splitting at significant variance with their results.

In this Comment, we will describe measurements made using two experimental systems. Both use laser-induced fluorescence on collimated atomic beams. In one experimental configuration, we use a fast atomic beam. It is generated by heating a solid Yb sample to 500 °C. The beam passes through a microcapillary array [10] and is further collimated after passing through a 12 mm aperture farther downstream. This configuration is similar to an older measurement by the DN group [11] and similar to what we used in a publication last year [12]. In the other experimental configuration, we reproduce the optical molasses setup of DN to generate a slow (20 m/s) isotopically pure atomic beam. Our molasses laser beam has a power of 1.1 W and an intensity of 1.4 W/cm^2. Our probe laser beam is generated using an independent laser. We also use a fixed-frequency laser beam tuned to the $F' = 5/2$ transition to address the optical pumping problem, which we describe below.

II. THE OPTICAL PUMPING PROBLEM

We question the data shown in Fig. 2 of the DN paper. That figure shows fluorescence measurements from the ^{173}Yb $F' = 3/2$ and $F' = 7/2$ levels in an isotopically pure, slow ^{173}Yb beam. Their probe laser beam size is 8 mm. The intensity of that laser beam ranges from about 0.3 to 0.5 times the saturation intensity. Rate equations show that optical pumping populates the ground state $m_F = \pm 5/2$ level after only 1 μs. Because the atoms spent 80 μs interacting with the laser beam, the $F' = 3/2$ transition should have been completely dark.

We show this in our optical molasses measurements. In Fig. 1, we show that in a nearly exact repeat of the DN measurement as they described it, there is no peak from the $F' = 3/2$ level. The only peak that is visible is from the $F' = 7/2$ level.

In our experiment, we address the optical pumping problem by introducing another laser beam into the interaction region. This additional laser is tuned to the $6s^2\ ^1S_0(F = 5/2) - 6s6p\ ^1P^o_1(F' = 5/2)$ transition, approximately 840 MHz below the $F' = 7/2$ transition. This laser scrambles the population in the lower m_F levels. When this laser is present, fluorescence from the $F' = 3/2$ level can be readily measured, as shown in Fig. 1.

We also note that the fluorescence levels shown in Fig. 2(c) of the DN paper appear to be in error. That figure shows 100% deflection of ^{172}Yb in the fast atomic beam. However, their optical molasses only addresses atoms with velocities less than 25 m/s. Given that the thermal velocity of their atoms is $v_{th} = (k_B T/m)^{1/2} = 165$ m/s, one would expect only $(\pi/18)^{1/2}(25/165)^3 = 0.15\%$ of the ^{172}Yb atoms to be deflected.

*scott.bergeson@byu.edu

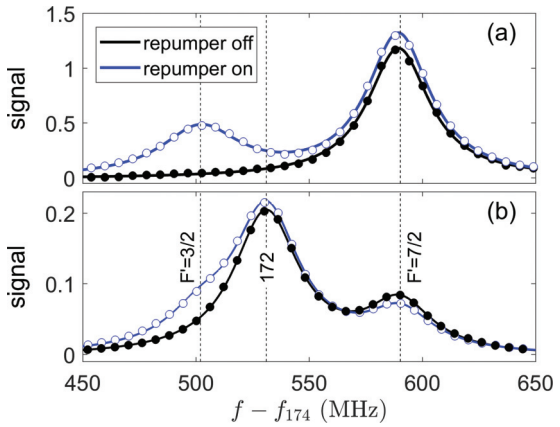

FIG. 1. Fluorescence measurements from (a) an isotopically pure, slow ^{173}Yb atomic beam and (b) a fast thermal beam. Without the repumper laser tuned to the $F' = 5/2$ transition (black circles), fluorescence from the $F' = 3/2$ level is completely absent. The repumper laser makes fluorescence from the $F' = 3/2$ level easily visible. The solid lines in this plot are fits to line-shape models including one, two, or three Lorentzian peaks, as appropriate.

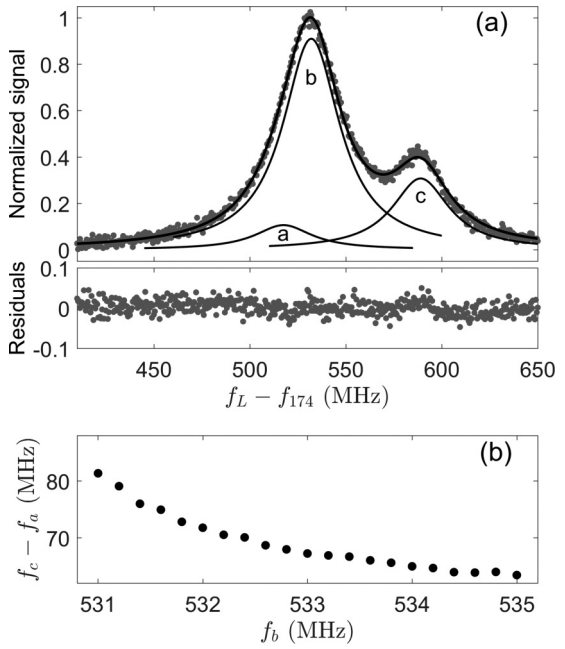

FIG. 2. Simulated data for the ^{172}Yb/^{173}Yb complex at 399 nm showing the critical error made in the analysis of Ref. [11]. (a) The computer generates a noisy line shape consisting of two partially resolved Lorentzians with center frequencies at 531 and 589 MHz. The dots are the simulated data; the solid line is a three-Lorentzian fit. The middle panel shows the residuals to the fit. In the model, the peak at 531 MHz is somewhat broader than the peak at 589 MHz. When the center frequencies for peaks "b" and "c" are fixed, a pseudopeak "a" appears in the fit. (b) The frequency difference between peak "c" and the pseudopeak "a" as a function of the "fixed" frequency for peak "b." Typical 1σ statistical uncertainties in determining the center frequency in repeated simulations are in the 0.3 MHz range. Dividing this by the square root of, say, 25 measurements reduces the *statistical* uncertainty in determining the line center to 0.06 MHz.

Optical pumping should have made measurement of the $F' = 3/2$ level impossible in the experiment of DN. It is not clear how the DN data could have been obtained given the information in their paper.

III. METROLOGY AND SPECTROSCOPY PROBLEMS

The group of DN has published many atomic transition frequency measurements over the past several years. As we pointed out in an earlier publication, their absolute transition frequencies in Yb [12] and K [13] have been shown to be in error by ∼500 MHz, in spite of estimated error bars of tens of kHz. Measurements in Rb [14] and Li [15] deviate from frequency-comb measurements in the MHz range, again in spite of estimated error of tens of kHz. In all cases, issues such as quantum interference in hyperfine spectroscopy [12,16] have been neglected by them, leading to additional MHz-level errors.

Recently, the group of DN has acknowledged that their spectroscopy method has been the likely cause of errors in isotope shift and hyperfine splitting measurements [17]. In many of their papers, they dithered their laser by 10 MHz while monitoring the fluorescence from their atomic samples. They demodulated the fluorescence signal at the third harmonic of the dither frequency to obtain a dispersion-shaped error signal. They locked their lasers to the zero crossing of this error signal. Any dc-offset errors are mapped directly into a frequency error. In a recent paper, the group of DN showed that this effect was the cause of a 4.5 MHz error in the ^{87}Rb $5P_{1/2}$ D1 hyperfine splitting [17].

As for the 2007 DN paper [9], we point out an additional error in the metrology. The spectra published in Fig. 2(b) of DN show that the $F' = 3/2,7/2$ splitting is over 80 MHz, disagreeing with their final result of 72.093 ± 0.036 MHz. This is readily verified by extracting their data using a program such as WEBPLOTDIGITIZER and fitting to a two-Lorentzian line-shape model. DN admit that this spectrum was not the one used to determine the splitting because they used the method described in the previous paragraph. This was necessary because their acousto-optic modulators (AOMs) did not have enough bandwidth to tune across the line profile. Interestingly, the data in Fig. 2(b) of the 2007 DN paper were obtained by scanning a separate laser over the line profile; the improved method used their correction of the ^{87}Rb $5P_{1/2}$ D1 hyperfine splitting [17].

The laser metrology and atomic spectroscopy methods used by DN are problematic and have been shown in some cases to be in error. The Yb spectrum published by DN does not agree with their final result [9]. Their final result does, surprisingly, match previous measurements from their own group [11,18]. It is to these measurements that we now turn our attention.

IV. PSEUDOPEAKS FROM ERRONEOUS LINE FITTING

In two earlier experiments, the group of DN measured laser-induced fluorescence from Yb atoms in a fast collimated atomic beam [11,18]. When the laser was scanned across the ^{172}Yb/^{173}Yb complex at 399 nm, they observed two peaks. The dominant one they correctly attributed to ^{172}Yb. The smaller one they correctly attributed to ^{173}Yb ($F' = 7/2$).

When they fit this signal to a two-Lorentzian line-shape model, they noticed that the ^{172}Yb peak was 1.3 times the width of the ^{173}Yb ($F' = 7/2$) peak. They hypothesized that this was due to the presence of the ^{173}Yb ($F' = 3/2$) component at a somewhat lower frequency. They then analyzed their data using a line-shape model with three Lorentzians, requiring the width of all three Lorentzians to be the same. Critically, they fixed the frequencies of the ^{172}Yb and ^{173}Yb ($F' = 7/2$) transitions and allowed the frequency of the lesser component to be a fit parameter. This artificially forces a peak to appear.

We show the unsuitability of this fitting procedure using a computer simulation. We simulate their data analysis by generating a Lorentzian peak at 531 MHz and a Lorentzian peak at 589 MHz, the approximate positions of the ^{172}Yb and ^{173}Yb ($F' = 7/2$) transitions (see Fig. 2). We add pseudorandom noise with an rms value of 1.5%. The simulated ^{172}Yb peak has a Lorentzian full width of 39 MHz. The simulated ^{173}Yb ($F' = 7/2$) peak has a Lorentzian full width of 30 MHz, similar to what was observed in Ref. [11]. We fit this simulated data to a three-Lorentzian line-shape model, fixing the frequencies of the ^{172}Yb and ^{173}Yb ($F' = 7/2$) transitions, and requiring the widths of all three peaks to be the same.

To show the error in this fitting procedure, we vary the frequency of the ^{172}Yb peak in the model. This forces a third peak to appear. In Fig. 2(b), we show the frequency of the pseudopeak as a function of the frequency of the ^{172}Yb peak in the model. As can be readily seen, a very good fit can be obtained with a shift that corresponds to the published data of Ref. [11] if one carefully chooses the "correct" frequency for ^{172}Yb. This simulation shows that the analysis used in the paper of Ref. [11] (and also Refs. [18] and [19]) is completely unfounded. The fact that the results of DN agree with this earlier publication in spite of the many concerns listed above is remarkable and surprising.

V. FREQUENCY-COMB MEASUREMENTS

We now present our measurements of the ^{173}Yb $F' = 3/2$ and $F' = 7/2$ levels. We have measured fluorescence from these levels in a fast thermal atom beam with the Yb isotopes in their natural abundances and also using an isotopically pure beam of slow ^{173}Yb atoms. In both cases, we used a pump laser beam tuned to the $F' = 5/2$ level to overcome the optical pumping problem discussed previously. The pump and probe beams are orthogonally polarized. They are combined on a polarizing beam-splitter cube before traversing the atomic beam. The pump and probe beam intensities are less than 1.5 mW/cm^2.

In our measurements, these weak probe laser beams cross a collimated Yb atomic beam at a right angle [12]. We collect scattered laser photons in a direction orthogonal to both the laser-propagation direction and the atomic-beam direction. We offset-lock our probe laser to an optical frequency comb [20,21]. We have shown that the absolute frequency error in our experiment is less than 40 kHz [12]. In the fast-beam measurements, the interaction region is enclosed in a single-layer mu-metal shield to minimize the influence of ambient magnetic fields on our measurements. In the slow-beam measurements, the lasers are retroreflected.

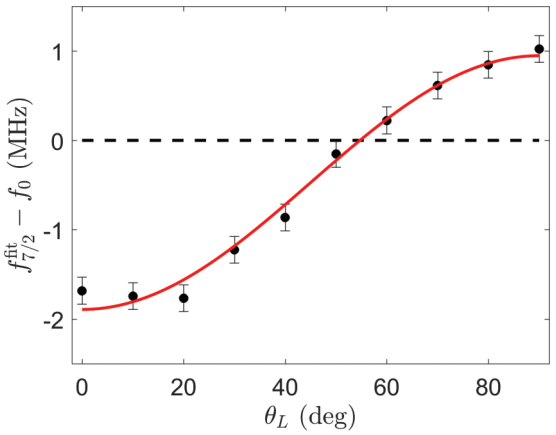

FIG. 3. Measurements of the apparent transition frequency for the $F' = 7/2$ peak as a function of the polarization angle, θ_L. Quantum interference in the excitation and decay pathways shifts the peak. Measurements made at $\theta_L = 54.7^\circ$ eliminate this effect.

For convenience, we will define the fluorescence collection direction as the $\hat{z}$ axis and measure the laser polarization angle θ_L with respect to that axis, as in previous work [12,16]. Because the pump and probe polarizations are orthogonal to each other, we will only refer to the polarization of the probe beam. A half-wave plate located before the vacuum chamber is used to rotate the polarization of both the pump and probe laser beams. This allows us to assess the influence of quantum interference on the apparent centers of the transitions [16]. For some measurements, we use a chopper wheel in the pump beam and phase-sensitive detection to eliminate background signal, for example, from the ^{172}Yb isotope.

Quantum interference in the excitation and decay pathways can shift the frequency of line centers measured in fluorescence spectroscopy [12,16]. Our measured frequencies of the $F' = 7/2$ level in ^{173}Yb are shown in Fig. 3. As we rotate the laser polarization angle, we see a 3 MHz shift in the transition frequency. We see a somewhat larger shift but with opposite sign in the $F' = 3/2$ transition. The measurements account for this shift by setting $\theta_L = \cos^{-1}(3^{-1/2}) = 54.7^\circ$, where the quantum interference terms vanish.

Based on these frequency-comb measurements, we report the frequencies of the ^{173}Yb $6s^2\ ^1S_0 - 6s6p\ ^1P^o_1(F' = 3/2)$ and $(F' = 7/2)$ transitions, relative to ^{174}Yb, to be

$$6s^2\ ^1S_0 - 6s6p\ ^1P^o_1(F' = 3/2) \quad 503.22 \pm 0.70 \text{ MHz},$$
$$6s^2\ ^1S_0 - 6s6p\ ^1P^o_1(F' = 7/2) \quad 589.51 \pm 0.33 \text{ MHz}. \quad (1)$$

This value of $F' = 7/2$ is consistent with our previous measurement [12], differing by less than one standard deviation. The frequency splitting between these two hyperfine levels is 86.29 ± 0.77 MHz.

VI. COMPARISON WITH THE LITERATURE

We calculate the hyperfine constants for ^{173}Yb using the Hamiltonian in Ref. [22] and also the $F' = 5/2$ data from Ref. [12]. Our values are given in Table I and compared with values from the literature.

TABLE I. Reported hyperfine constant values from the literature for the ^{173}Yb $6s6p\ ^1P_1^o$ level.

Method	Year	A_{173} (MHz)	B_{173} (MHz)
This work	2017	59.52 ± 0.20	601.87 ± 0.49
Beam [19]	2010	57.9 ± 0.2	608.4 ± 0.8
Molasses [9]	2007	57.693 ± 0.006	609.028 ± 0.056
Beam [11]	2005	57.682 ± 0.029	609.065 ± 0.098
Beam [18]	2003	57.91 ± 0.12	610.47 ± 0.84
Beam [23]	2002	57.7 ± 0.9	602.1 ± 1.1
Level crossing[a] [24]	1985	58.1 ± 0.3	588 ± 2
Level crossing [25]	1976	58.45 ± 0.80	589.6 ± 13.0
Level crossing [26]	1969	56.9 ± 0.50	575 ± 7

[a]Additional optical pumping was used in this experiment.

Laser-spectroscopy measurements for ^{173}Yb are reported in Refs. [9,11,18,19,23]. The group of DN published values with the smallest error estimates in Table I [9,11,18] and we question these publications in this comment. The analysis in Ref. [19] follows the unfortunate analysis of the DN group, which we have shown in Sec. IV to be prone to significant systematic error. None of the values in the literature address the quantum interference in the $F' = 7/2$ level. None of them address the influence of optical pumping for the $F' = 3/2$ fluorescence level. In the atomic beam data of Refs. [11,18,19], the $F' = 3/2$ component is invisible.

The laser-spectroscopy measurement of Ref. [23] used a different approach. They measured fluorescence from an atomic beam of Yb atoms with the laser polarized at $\theta_L = 0$ and $\theta_L = 90^\circ$. In the $\theta_L = 0$ measurement, the fluorescence signal is dominated by fluorescence from the highly abundant even isotopes. In the $\theta_L = 90^\circ$ fluorescence measurement, the even isotopes are strongly suppressed compared to the odd isotopes because of the dipole radiation pattern. The small residual fluorescence from the even isotopes can be subtracted out using an appropriate scaling of the $\theta_L = 0$ data. From the hyperfine constants in Ref. [23], we calculate a hyperfine splitting between the ^{173}Yb $F' = 7/2$ and $3/2$ levels to be 75.3 ± 4.0 MHz. This $\theta_L = 0$ measurement needs to be corrected for the quantum interference effect. Our measurements suggest this is approximately 5 MHz, making their measurement a little over 80 MHz with an uncertainty of 4 MHz. This interval differs from our measurement by just under two standard deviations.

ACKNOWLEDGMENT

We acknowledge support from the National Science Foundation under Grant No. PHY-1500376 and from the Air Force Office of Scientific Research under Grant No. AFOSR-FA9550-17-1-0302.

[1] V. A. Dzuba, W. R. Johnson, and M. S. Safronova, Phys. Rev. A **72**, 022503 (2005).
[2] J. J. Cowan and C. Sneden, Nature (London) **440**, 1151 (2006).
[3] J. Ginges and V. Flambaum, Phys. Rep. **397**, 63 (2004).
[4] D. Antypas, A. Fabricant, L. Bougas, K. Tsigutkin, and D. Budker, Hyperfine Interact. **238**, 21 (2017).
[5] V. V. Flambaum, V. A. Dzuba, and C. Harabati, Phys. Rev. A **96** 012516 (2017).
[6] X. Zheng, Y. R. Sun, J.-J. Chen, W. Jiang, K. Pachucki, and S.-M. Hu, Phys. Rev. Lett. **118**, 063001 (2017).
[7] C. Frugiuele, E. Fuchs, G. Perez, and M. Schlaffer, Phys. Rev. D **96**, 015011 (2017).
[8] S. G. Porsev, Y. G. Rakhlina, and M. G. Kozlov, J. Phys. B **32**, 1113 (1999).
[9] D. Das and V. Natarajan, Phys. Rev. A **76**, 062505 (2007).
[10] R. Senaratne, S. V. Rajagopal, Z. A. Geiger, K. M. Fujiwara, V. Lebedev, and D. M. Weld, Rev. Sci. Instrum. **86**, 023105 (2015).
[11] D. Das, S. Barthwal, A. Banerjee, and V. Natarajan, Phys. Rev. A **72**, 032506 (2005).
[12] M. Kleinert, M. E. Gold Dahl, and S. Bergeson, Phys. Rev. A **94**, 052511 (2016).
[13] S. Falke, E. Tiemann, C. Lisdat, H. Schnatz, and G. Grosche, Phys. Rev. A **74**, 032503 (2006).
[14] M. Maric, J. J. McFerran, and A. N. Luiten, Phys. Rev. A **77**, 032502 (2008).
[15] C. J. Sansonetti, C. E. Simien, J. D. Gillaspy, J. N. Tan, S. M. Brewer, R. C. Brown, S. Wu, and J. V. Porto, Phys. Rev. Lett. **107**, 023001 (2011).
[16] R. C. Brown, S. Wu, J. V. Porto, C. J. Sansonetti, C. E. Simien, S. M. Brewer, J. N. Tan, and J. D. Gillaspy, Phys. Rev. A **87**, 032504 (2013).
[17] D. Datar, N. Kotibhaskar, S. Ananthamurthy, and V. Natarajan, arXiv:1611.02406.
[18] A. Banerjee, U. D. Rapol, D. Das, A. Krishna, and V. Natarajan, Europhys. Lett. **63**, 340 (2003).
[19] W. Wen-Li and X. Xin-Ye, Chin. Phys. B **19**, 123202 (2010).
[20] P. Fendel, S. D. Bergeson, T. Udem, and T. W. Hänsch, Opt. Lett. **32**, 701 (2007).
[21] M. Lyon and S. D. Bergeson, Appl. Opt. **53**, 5163 (2014).
[22] E. Arimondo, M. Inguscio, and P. Violino, Rev. Mod. Phys. **49**, 31 (1977).
[23] R. Zinkstok, E. J. van Duijn, S. Witte, and W. Hogervorst, J. Phys. B **35**, 2693 (2002).
[24] H. Liening, Z. Physik. A **320**, 363 (1985).
[25] M. Baumann, H. Liening, and H. Lindel, Phys. Lett. A **59**, 433 (1977).
[26] B. Budick and J. Snir, Phys. Rev. **178**, 18 (1969).

Applied Radiation and Isotopes 142 (2018) 113–119

Contents lists available at ScienceDirect

Applied Radiation and Isotopes

journal homepage: www.elsevier.com/locate/apradiso

2.7 years of beta-decay-rate ratio measurements in a controlled environment

Q. McKnight, S.D. Bergeson*, J. Peatross, M.J. Ware

Department of Physics and Astronomy, Brigham Young University, Provo, UT 84602, United States

HIGHLIGHTS

- A series of publications beginning in 2009 hypothesizes that nuclear decay rates depend on solar activity. If true, this controversial claim points to new physics outside the standard model. Solar-dependent variations would invalidate the purely exponential decay of radioactive nuclei, potentially requiring modifications to radiation standards, with important implications for geo- and astrochronology. If nuclear decay rate variations are related to the solar neutrino flux, for example, measured variations could be used to detect neutrinos or to measure or predict solar flares.
- Since the first papers were published, dozens of published research articles have studied this effect. Some affirm solar-related variations while others refute them. One key commonality in all pro-variation papers is that the detectors are used in an un-controlled ambient environment. The local temperature and pressure change with the weather and seasons. Our work is among the few studies in which the ambient environment is tightly controlled. The sealed, temperature-controlled, low-humidity environment has been nearly un-interrupted and acquiring data for 2.7 years.
- Noisy data, even truly random data, can exhibit small-amplitude periodicities. For example, a Sr/Y data set was published a few years ago. The scientists who generated the data performed a detailed analysis showing that there was no statistically-significant evidence for solar-related variation. This same data set was analyzed by a separate group that claimed to find an indication of Solar-correlated variation. In our present work, we show that such small amplitude "positive" periodicity results can be obtained from pseudo-random noise.
- Finally, we demonstrate how ratio-calibration methods are not as reliable as one might like. Our data illustrates how long-term drifts in both the absolute and relative detection efficiency can masquerade as "interesting" science if systematic effects are not properly considered.
- Our work confirms a null-variability measurement, competitive with the best measurements produced by national standards labs. It illustrates the limits of accuracy and sensitivity for these detector types. We suggest that reducing the limit significantly will require perhaps a new generation of detectors.

ARTICLE INFO

Keywords:
Nuclear decay rate measurements
Beta decay
Decay rate variability
Nuclear decays
Half-life
Decay constant
Non-exponential decay
Radioactivity

ABSTRACT

We report nearly continuous beta-decay-rate measurements of Na-22, Cl-36, Co-60, Sr-90, and Cs-137 over a period of 2.7 years using four Geiger-Müller tubes. We carefully control the ambient pressure and temperature for the detectors, sources, and electronics in order to minimize environmentally-dependent systematic drifts in the measurement chains. We show that the amplitudes of an annual oscillation in the decay rates are consistent with zero to within 0.004%.

1. Introduction

In a series of articles, Pommé et al. argue against the hypothesis that nuclear decay rates depend on the Earth-Sun distance or on solar activity (Pommé et al., 2016, 2017a, 2017b, 2017c, 2018a). These articles analyzed data spanning several decades in time collected by 14 national standards laboratories measuring 20 different radioactive isotopes. Collectively, they set an upper limit of 0.003–0.007% in the amplitude of annual oscillations in the measured beta decay rates (Pommé et al., 2017b) and similar limits for alpha and beta$^+$ decay rates. Many other publications agree with these findings (Bellotti et al., 2018; Borrello et al., 2018; Bergeson et al., 2017a; Cooper, 2009; Kossert and Nähle, 2015, 2014; Meier and Wieler, 2014; Nähle and Kossert, 2014; Norman et al., 2009; Schrader, 2016).

Nuclear radiation detectors are known to be influenced by their operating environment (Bergeson et al., 2017a; Bergeron et al., 2018; Schrader, 2016; Siegert et al., 1998; Stancil et al., 2017; Ware et al., 2015), and these systematic variations can masquerade as interesting

* Corresponding author.
E-mail address: scott.bergeson@byu.edu (S.D. Bergeson).

https://doi.org/10.1016/j.apradiso.2018.09.021
Received 2 July 2018; Received in revised form 14 September 2018; Accepted 17 September 2018
Available online 20 September 2018

science. For example, a recent publication observed solar-correlated changes in the measured ^{222}Rn decay rate (Sturrock et al., 2018). That study used multi-year data from an outdoor monitoring station. When the study was repeated in a laboratory environment, no oscillations were observed (Pommé et al., 2018b). The reported decay-rate-variations appear to be a systematic effect related to the detector temperature (Pommé et al., 2018b). Similarly, solar-correlated variations were previously observed in ^{54}Mn (Fischbach et al., 2009), ^{36}Cl (Jenkins et al., 2012), and other elements. However measurements performed by us and many others in carefully controlled ambient environments and using stabilized detectors show no variability at levels well below what was originally reported (Bellotti et al., 2018; Bergeson et al., 2017a; Borrello et al., 2018; Kossert and Nähle, 2015, 2014; Nähle and Kossert, 2014; Norman et al., 2009; Pommé et al., 2016; Schrader, 2016).

The search for new science outside the standard model is a staple of physics research (Safronova et al., 2018). Unresolved questions about dark matter and dark energy (Spergel et al., 2003; Planck Collaboration et al., 2014), the proton size (Udem, 2018), the magnetic moment of the muon (Belyaev et al., 2018; Bauer et al., 2017; Chakraborty et al., 2018), tensor gravity (García-Bellido and Quirós, 1990; Steinwachs and van der Wild, 2018), and temporal variations of the fundamental "constants" (Martins, 2017) inspire studies of axion coupling to normal matter, primordial black holes, sterile neutrinos, and searches for higher-dimensional space, to name a few examples. While these studies are not always successful, they contribute to a growing body of science and remind us that nature sometimes holds surprises.

Even though the link between solar activity and possible variations in nuclear beta decay rates has been disproven at the 0.007% level, the question of the stability of nuclear decay is interesting to consider. In this paper we report an extension of our previous beta-decay-rate measurements to a period of 2.7 years. Our data places an upper limit of 0.004% for the amplitude of an annual oscillation in the decay rate, which appears to be near the limit of accuracy for Geiger-Müller (GM) beta detectors. We show that counting statistics and long-term detector drift pose significant systematic errors below this level of precision.

2. Data acquisition

Our experiment is described in previous publications (Bergeson et al., 2017a; Ware et al., 2015). Five 1-μCi samples (Na-22, Co-60, Sr-90, Cs-137, and Cl-36) and a blank are mounted in a bismuth-lined sample holder. A closed-loop feedback-controlled rotation stage sequentially rotates the samples into position above four GM tubes, with an accuracy of $\pm$ 10 μm. The samples, rotation stage, detectors, and associated electronics are placed in a sealed chamber containing dry nitrogen. The chamber pressure and wall temperature are controlled to be 93.33 kPa (700 Torr) and 32.2 °C (90 °F).

Plastic apertures in front of each sample limit the GM count rate to approximately 400 counts per second (cps) when the experiment was started. Typical background signals are 0.4 cps. Each sample is measured for a period of 4 h each day. We average the count rate over 14 days to get one data point. The statistical uncertainty in each data point is expected to be $\sigma = [(400\ \text{counts/s})(14,\ 400\ \text{s/d})(14\ \text{d})]^{-0.5} = 1.1 \times 10^{-4}$.

The data reported here were acquired between 17 September 2015 and 4 June 2018 (992 days). Because the fractional count rate change with pressure is 10^{-4} Torr^{-1}, data is discarded when the chamber is opened and the pressure is uncontrolled, Data is also discarded when rotation stage positioning errors are reported. One of the four detectors failed during the experiment, limiting the available data for that detector. Additional information on the detectors and data filtering is presented in the Appendix A.

3. Data reduction

Our raw count-rate data is corrected for dead time, using

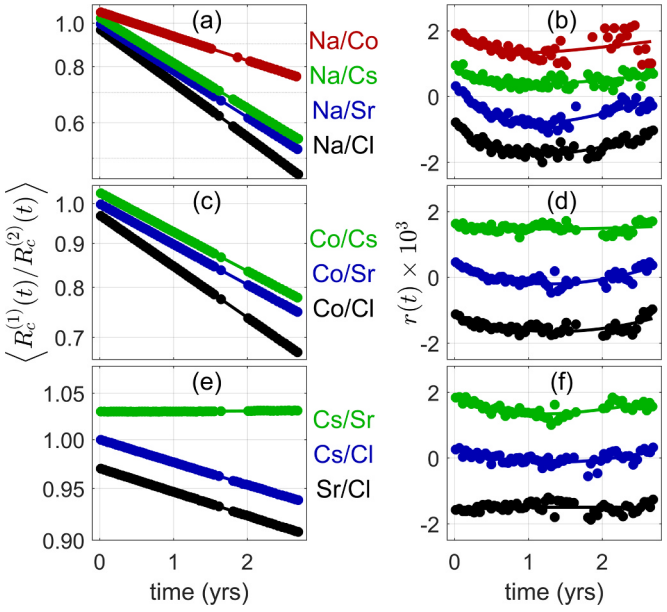

Fig. 1. Normalized averaged count rate ratios. The count rate ratios from each detector are averaged together as described in the text. In panels (a), (c), and (e), the circles are the ratio data and the lines represent the exponential best fit to the data. In panels (b), (d), and (f), the points are the residuals $r(t)$ calculated using Eq. (4) and the lines are the detrending function from Eq. (5). The elements used in the count rate ratios are listed to the right of panels (a), (c), and (e) as follows. Panels (a) and (b): Na/Co, red; Na/Cs, green; Na/Sr, blue; Na/Cl, black. Panels (c) and (d): Co/Cs, green; Co/Sr, blue; Co/Cl, black. Panels (e) and (f): Cs/Sr, green; Cs/Cl, blue; Sr/Cl, black. (For interpretation of the references to color in this figure legend, the reader is referred to the web version of this article.)

$$R_c(t) = \frac{R_m(t)}{1 - R_m(t)\,\tau} - B_m(t), \tag{1}$$

where R_m is the measured count rate, R_c is the dead time-corrected count rate, τ is the dead time, approximately 200 μs, and B_m is the measured background level for the detector. The corrected count rates for our 5 samples are used to generate 10 unique count rate ratios for each of the 4 detectors. As shown in the Appendix A [Fig. 4(a)], these count rate ratios do not have exactly the same values at time $t = 0$. Furthermore, the count rate ratio data are comprised of different numbers of days on each detector due to the data filtering mentioned previously. We normalize the count rate ratios for each detector using the average of the first 400 days. On a given day, we average the ratio data using all detectors for which the data is valid. These ratio data are plotted in Fig. 1(a), (c), and (e).

In the absence of detector errors and source variability, the count rates should follow simple exponential decay. Although our environmental control eliminates some sources of systematic error related to detector response variability, the detectors themselves age over time. Common-mode drift in the detector response can be minimized by calculating decay rate ratios, although even then artifacts remain (Towers, 2013). Details and an illustration from our data are given in the Appendix A. The ratio data are fit to a single exponential decay. The idealized count rate ratio should be,

$$\frac{R_c^{(1)}(t)}{R_c^{(2)}(t)} = A \exp\left(-\lambda t\right), \tag{2}$$

where the superscripts (1) and (2) refer to the elements in the count rate ratio, A is the count rate ratio at time $t = 0$, and λ is the decay rate. We linearize this in the usual way as

$$\ln\left(\frac{R_c^{(1)}(t)}{R_c^{(2)}(t)}\right) = \ln(A) - \lambda t, \tag{3}$$

and use $\ln(A)$ and λ as fit parameters. These fits are plotted with the count rate ratios in the left-hand panels of Fig. 1. The fitted decay rates reproduce known rates with an error of typically 0.0006 per year (Bergeson et al., 2017a).

Residuals to the single-exponential decay fit are calculated as

$$r(t) = \frac{R_c^{(1)}(t)}{R_c^{(2)}(t)} \frac{1}{R_{\text{fit}}(t)} - 1, \tag{4}$$

where $R_{\text{fit}}(t)$ is the least-squares exponential decay fit. These residuals are shown in the right-hand panels of Fig. 1. Long-term drifts in the detector response are readily observable (see Appendix A).

To remove residual long-term drift in the ratios, we use a phenomenological drift function,

$$d(t) = a\exp(-\gamma t) + bt + c, \tag{5}$$

where a, b, c, and γ are fit parameters. The solid lines shown in panels (b), (d), and (f) of Fig. 1 show the least-squares-fit detrending functions for all of the count rate ratios. Using numerical simulations, we verify that detrending reduces the amplitude of a small annual oscillation by only 15%. Its influence on higher frequency variations is even less pronounced. As we discuss in Section 4, this has a negligible effect on the search for seasonal variation in the decay rate. Relative to the detrending function, the average standard deviations of the residuals is 2.1×10^{-4}. This is near the expected value for the ratio of two measurements, each with a count rate of 400 cps measured 4 h per day and averaged over 14 days.

4. Analysis

The detrended residuals are calculated as

$$r_2(t) = r(t) - d(t), \tag{6}$$

and are plotted in Fig. 2. Annual or seasonal variations in the nuclear decay rate, if they exist, should appear in the detrended residuals. The

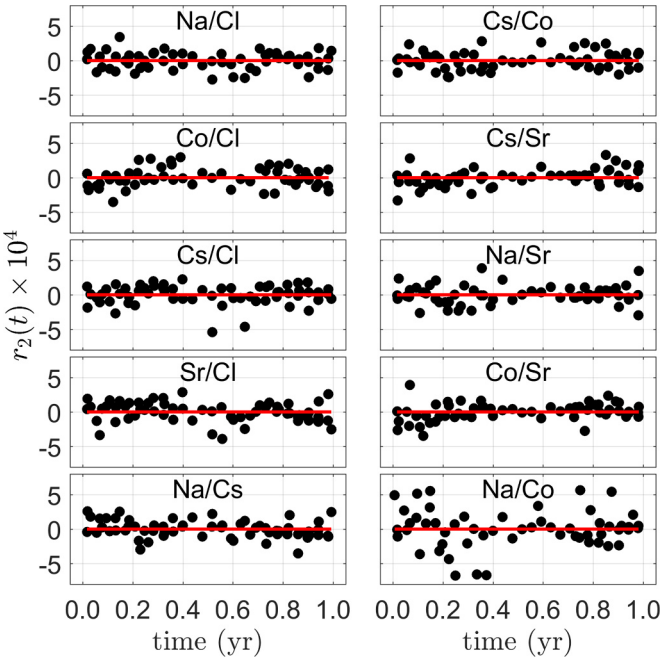

Fig. 2. Detrended residuals, $r_2(t)$, as defined in Eq. (6), for 10 unique beta-decay-rate ratios. Also shown is a cosine fit with its amplitude and phase. The entire 2.7 year data set is included in these plots, with the data plotted as a function of the day of the year. The zero of time is January 1.

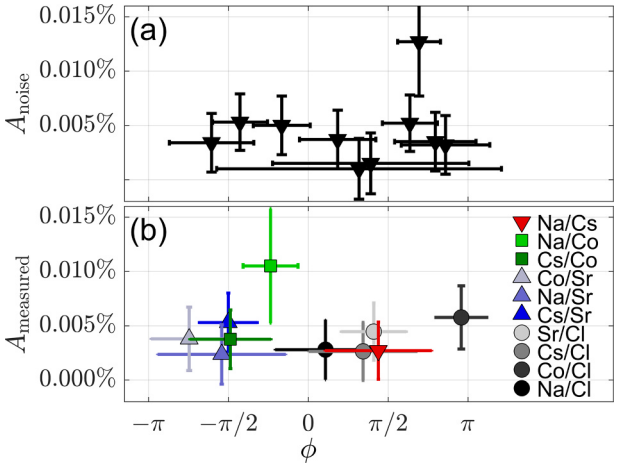

Fig. 3. The amplitude and phase obtained by fitting the detrended count-rate ratios to Eq. (7). (a) We extracted fits from pseudo-random noise with noise characteristics similar to our measured detrended ratios. Typical "amplitudes" from this purely Gaussian noise are 0.004%. (b) Fits from our actual data. The actual data gives similar fit values as the pure noise. The fitted amplitudes are consistent with zero at the level of 0.004%.

zero of time corresponds to January 1. The 2.7-year data records are plotted versus the day of the year. Also shown is a fit to a cosine function with a 1-year period,

$$y(t) = A\cos(2\pi t - \phi), \tag{7}$$

with A and ϕ as free parameters. As can be seen in Fig. 2, the fits are essentially flat with amplitudes well below the rms noise. For these 10 ratios, the average of the fit amplitude is 4×10^{-5}, with a standard deviation of 2×10^{-5}. The fit amplitudes are plotted in Fig. 3b and range from 1.0×10^{-5} to 5.7×10^{-5}.

We assess the reliability of the fits in two ways. In the first method, we generate Gaussian pseudo-random data with an rms width of 1.5×10^{-4} for $N = 62$ data points equally spaced over a 1 year interval and fit that data to a cosine function using Eq. (7). In 1000 repeated trials, the average of the fitted amplitude (magnitude) is 4×10^{-5}, with a standard deviation of 2×10^{-5}. This exactly matches the fits to our real data, suggesting that the fitted amplitudes from the measured data are consistent with zero.

In the second method, we perform a traditional least-squares fit to a cosine function. The χ-squared parameter is calculated using

$$\chi^2 = \sum \left\{\frac{1}{\sigma_i^2}[y_i - y(x_i)]^2\right\}, \tag{8}$$

where $y(x_i)$ is calculated using Eq. (7), y_i is the detrended residuals in the count-rate ratio, and σ_i is the standard deviation of the detrended fit residuals. We generate a grid in the space of A and ϕ and calculate χ^2 at every point in that grid. Near the region of the minimum, we fit the surface to a parabola. The uncertainty in the fit parameter is defined to be the value that increases the value of χ^2 by 1 (Bevington and Robinson, 2003). For the Na/Cl ratio, for example, using $\sigma_i = 1.5 \times 10^{-4}$, the amplitude and phase are $A = (2.8 \pm 2.8) \times 10^{-5}$ and $\phi = (0.3 \pm 1.0)$ rad. The standard error in the mean of the fit residuals of the Na/Cl ratio data is 1.6×10^{-5}. Across the 10 ratios, the standard error in the mean of the fit residuals is below 2.0×10^{-5}, with the exception of the Na/Co data where the standard error is 3.7×10^{-5}.

Continuing this analysis, we compare the amplitude and phase from fitting our detrended residuals to Eq. (7) to the results of fitting pseudo-random noise with similar noise characteristics as our data to Eq. (7). This comparison is shown in Fig. 3. It is clear that our data show no indication of an annual oscillation at the level of 0.004%. The amplitudes of the annual oscillations are consistent with zero at this level. Periodogram analysis searching for oscillations at higher frequencies

shows no peaks at 9.43 per year or 12.7 per year in any of the data. These frequencies correspond to known (Ashie et al., 2004; Desai and Liu, 2016) and speculated (Sturrock et al., 2013) variations in the solar neutrino flux (Pommé et al., 2017d).

5. Conclusion

We measure beta-decay rates of Na-22, Cl-36, Co-60, Sr-90, and Cs-137 using four GM detectors over a period of 2.7 years in a controlled environment. Common-mode detector drift is reduced using count-rate ratios for each detector, enabling cross-detector comparison. Long-term detector drift is further removed using a phenomenological detrending function. In our data, the amplitude of an annual oscillation in the decay rate is excluded at the 0.004% level for measured count rate ratios for all isotopes in the study. Spectral analysis reveals no peaks at 9.43 per year or 12.7 per year in any of the data.

In order to significantly reduce the uncertainty in beta-decay measurements, significant limitations need to be overcome. Generating data with better counting statistics would be helpful. However, standard GM tubes have deadtimes on the order of 200 μs. For a count rate of 500 cps, the dead-time correction is 10%. A careful analysis might reduce the uncertainty in the dead-time correction to a few tenths of a percent. However, artifacts at the 0.001% level and below are likely to remain, even in ratio measurements. It is possible to make measurements using an array of detectors. This would enable careful cross-checking of systematic errors. However, as we show in the Appendix A, detectors age at different rates, leading to changes in both the relative and absolute quantum yield for beta detection. With appropriate detrending, this might be a suitable pathway to better statistics. In some cases, gamma detection using NaI scintillation detectors can be stable enough to give null results up to a factor of 10 better than in beta-particle detectors (Bellotti et al., 2018). Here again, some issues need attention for high-stability measurements (Bergeson et al., 2017b).

Appendix A

Stabilizing the temperature and pressure for the detectors, samples, and electronics makes variations in the detector gain inherently small (Bergeson et al., 2017a; Ware et al., 2015). Computing the ratios of count rates using a single detector eliminates common-mode measurement artifacts, such as geometric factors, path-length differences, and some gain variability, as we show below. However, we also show that some kinds of detector drifts are not entirely common-mode and do not divide out in the ratio (Towers, 2013).

In Fig. 4(a) we show the deadtime-corrected count rates for the four detectors measuring Na-22. Breaks in the data correspond to detector failure of detector 2 at day 418, a computer operating system error (detectors 1 and 3, days 585–650), and positioning error (detector 4, days 435–941).

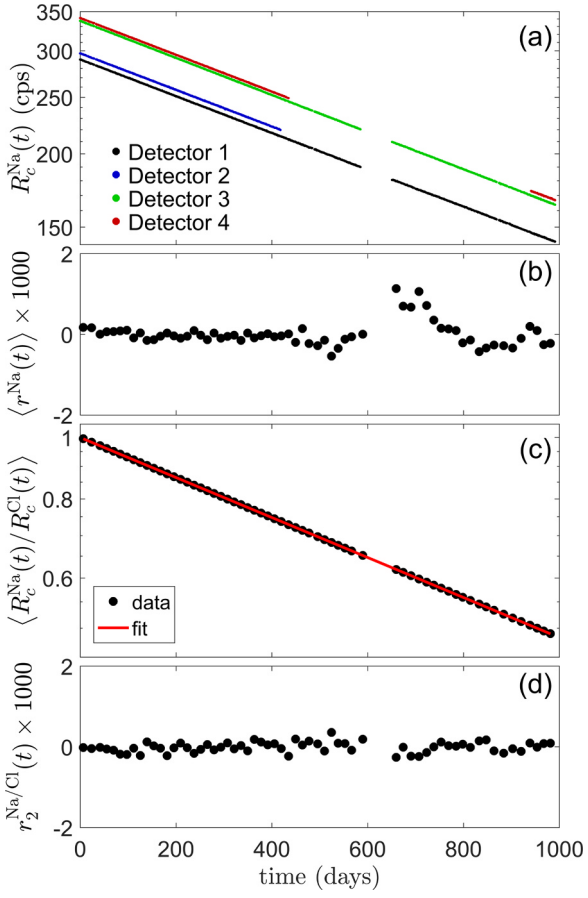

Fig. 4. (a) The deadtime-corrected count rate measurements of Na in each of the four detectors, without averaging. Detector 2 failed at day 418. The closed-loop feedback control failed for position 6 (detector 4 in this plot) at day 435 and was reset at day 941. The data acquisition system was interrupted from day 585–650 due to an error in the computer operating system. The experimental chamber was opened to replace detector 2 and the experiment was restarted at day 651. No data is shown for detector 2 after it failed, for reasons discussed in the text. (b) The average residuals to a single-exponential fit, calculated for each detector and then averaged together. The data are binned into 14 day intervals for clarity. Notice the 200 day drift back to the equilibrium value after the chamber was serviced at day 650. (c) The count rate ratio for Na divided by Cl, averaged over 14 days. (d) The detrended residuals, calculated using Eq. (6) for the Na/Cl ratio. The detector drift after day 650 in panel (b) is absent in panel (d).

Detector drift becomes apparent when the count rates are compared to best-fit single-exponential decay curves, as shown in Fig. 4(b). For this plot, each of the detectors was fit to an exponential decay curve, and the residuals from Eq. (4) are averaged together. This analysis uses only the Na-22 count rate data and not a count rate ratio. The residuals data are then binned into 14 day intervals to improve clarity. At the 0.1% level, the residuals for the first 600 days are small and nearly featureless. However, after the chamber was serviced at day 650, it takes nearly 200 days for the residuals to drift back to their previous value.

Calculating the ratio followed by detrending using Eqs. (4) and (6) improves the overall data, as shown in panels (c) and (d) of Fig. 4. Here the Na/Cl count rate ratio is computed for each detector and then averaged together. The data, fit, and detrended residuals from Eq. (6) are plotted. The 200-day-long drift after day 650 is now absent and the detrended residuals display no curvature.

The amount by which detector variation is suppressed in ratio calculations can be readily determined. At a particular time t, the measured count rates are proportional to the number of radioactive nuclei in our sample, N. To within multiplicative constants, a measurement of sample 1 can be represented as

$$m_1 = N_1\lambda_1 \exp(-\lambda_1 t)\mathscr{D}(t), \tag{9}$$

and a measurement of sample 2 can be represented as

$$m_2 = N_2\lambda_2 \exp(-\lambda_2 t)\mathscr{D}(t), \tag{10}$$

where $\mathscr{D}(t)$ is the time-dependent detector response. When the two measurements are separated by a time Δt, the ratio is

$$\frac{m_1}{m_2} = \frac{N_1\lambda_1}{N_2\lambda_2}\frac{\exp(-\lambda_1 t)}{\exp[-\lambda_2(t+\Delta t)]}\frac{\mathscr{D}(t)}{\mathscr{D}(t+\Delta t)} \tag{11}$$

For small values of Δt, we can write,

$$\frac{m_1}{m_2} \approx \left[\frac{N_1\lambda_1}{N_2\lambda_2}\frac{\exp(-\lambda_1 t)}{\exp(-\lambda_2 t)}\right]\exp\left(\lambda_2\Delta t\right)\left(1 - \frac{1}{\mathscr{D}}\frac{d\mathscr{D}}{dt}\Delta t\right). \tag{12}$$

The fractional variation in the detector response is suppressed by the factor Δt. In our data analysis, $\Delta t \leq 20$ h. Monotonic variations are further reduced using our detrending function. However, non-monotonic variation is problematic.

We observe non-monotonic detector variation in our measurements. Detector 2 failed at day 413 and was replaced with a new one at day 650. For a few hundred days after the new detector is installed, we observe drifts in both the absolute and the relative response of the GM tube to beta particles of different energy, as shown in Fig. 5. The measurements for Cl-36 are instructive. Because its half life is 302,000 years, we expect the count rate to be constant during our measurement period. On the old detector, a small but steady increase is visible in Fig. 5(a) prior to day 413. On the new detector, a short oscillation is observed after day 651 followed by a long slow decay. In Fig. 5(b), we see that the drift in the detector response is not cancelled when a ratio is calculated. Some of the drift is similar to what is observed in Fig. 4(b). However, sub-percent variation in the ratio is visible after day 651. The "offset" in the ratio after day 651 is positive for the Cs/Cl ratio. However, for some ratios the shift after day 651 is sometimes up and sometimes down. It appears to depend on the energy of the detected beta-particle and whether the detected particle is beta-plus or beta-minus. Detector response variation will need to be more carefully characterized and controlled for high-precision determinations of nuclear decay rates (Towers, 2013).

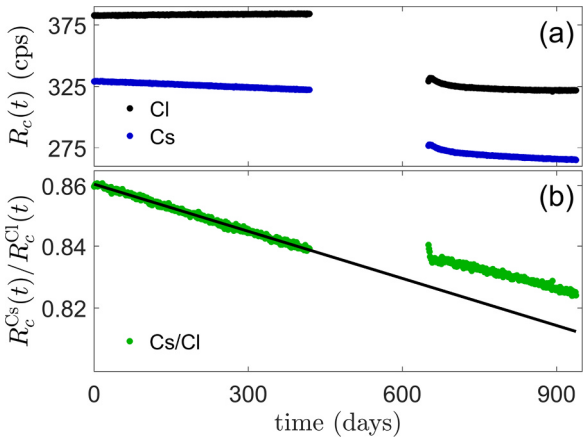

Fig. 5. Count rate ratios measured using detector 5. This detector replaced detector 2 when it failed. The deviation of the count rate ratio from the expected value is largest when the difference in the beta particle energies between the two samples in the ratio is greatest. Quantum efficiency differences between beta$^-$ and beta$^+$ are also observed.

References

Ashie, Y., Hosaka, J., Ishihara, K., Itow, Y., Kameda, J., Koshio, Y., Minamino, A., Mitsuda, C., Miura, M., Moriyama, S., Nakahata, M., Namba, T., Nambu, R., Obayashi, Y., Shiozawa, M., Suzuki, Y., Takeuchi, Y., Taki, K., Yamada, S., Ishitsuka, M., Kajita, T., Kaneyuki, K., Nakayama, S., Okada, A., Okumura, K., Ooyabu, T., Saji, C., Takenaga, Y., Desai, S., Kearns, E., Likhoded, S., Stone, J.L., Sulak, L.R., Walter, C.W., Wang, W., Goldhaber, M., Casper, D., Cravens, J.P., Gajewski, W., Kropp, W.R., Liu, D.W., Mine, S., Smy, M.B., Sobel, H.W., Sterner, C.W., Vagins, M.R., Ganezer, K.S., Hill, J., Keig, W.E., Jang, J.S., Kim, J.Y., Lim, I.T., Ellsworth, R.W., Tasaka, S., Guillian, G., Kibayashi, A., Learned, J.G., Matsuno, S., Takemori, D., Messier, M.D., Hayato, Y., Ichikawa, A.K., Ishida, T., Ishii, T., Iwashita, T., Kobayashi, T., Maruyama, T., Nakamura, K., Nitta, K., Oyama, Y., Sakuda, M., Totsuka, Y., Suzuki, A.T., Hasegawa, M., Hayashi, K., Inagaki, T., Kato, I., Maesaka, H., Morita, T., Nakaya, T., Nishikawa, K., Sasaki, T., Ueda, S., Yamamoto, S., Haines, T.J., Dazeley, S., Hatakeyama, S., Svoboda, R., Blaufuss, E., Goodman, J.A., Sullivan, G.W., Turcan, D., Scholberg, K., Habig, A., Fukuda, Y., Jung, C.K., Kato, T., Kobayashi, K., Malek,

M., Mauger, C., McGrew, C., Sarrat, A., Sharkey, E., Yanagisawa, C., Toshito, T., Miyano, K., Tamura, N., Ishii, J., Kuno, Y., Nagashima, Y., Takita, M., Yoshida, M., Kim, S.B., Yoo, J., Okazawa, H., Ishizuka, T., Choi, Y., Seo, H.K., Gando, Y., Hasegawa, T., Inoue, K., Shirai, J., Suzuki, A., Koshiba, M., Nakajima, Y., Nishijima, K., Harada, T., Ishino, H., Nishimura, R., Watanabe, Y., Kielczewska, D., Zalipska, J., Berns, H.G., Gran, R., Shiraishi, K.K., Stachyra, A., Washburn, K., Wilkes, R.J., 2004. Evidence for an oscillatory signature in atmospheric neutrino oscillations. Phys. Rev. Lett. 93, 101801. https://doi.org/10.1103/PhysRevLett.93.101801.

Bauer, M., Neubert, M., Thamm, A., 2017. LHC as an axion factory: probing an axion explanation for $(g-2)_\mu$ with exotic Higgs decays. Phys. Rev. Lett. 119, 031802. https://doi.org/10.1103/PhysRevLett.119.031802.

Bellotti, E., Broggini, C., Carlo, G.D., Laubenstein, M., Menegazzo, R., 2018. Search for time modulations in the decay constant of ^{40}K and ^{226}Ra at the underground Gran Sasso Laboratory. Phys. Lett. B 780, 61–65. https://doi.org/10.1016/j.physletb.2018.02.065.(URL ⟨http://www.sciencedirect.com/science/article/pii/S0370269318301771⟩).

Belyaev, A.S., King, S.F., Schaefers, P.B., 2018. Muon $g-2$ and dark matter suggest nonuniversal gaugino masses: $SU(5)\times A_4$ case study at the LHC. Phys. Rev. D 97, 115002. https://doi.org/10.1103/PhysRevD.97.115002.

Bergeron, D.E., Cessna, J.T., Zimmerman, B.E., 2018. Two determinations of the Ge-68 half-life, applied radiation and isotopes. In: Proceedings of the 21st International Conference on Radionuclide Metrology and its Application. ICRM 2017, 134, pp. 416–420. ⟨https://dx.doi.org/10.1016/j.apradiso.2017.10.038⟩. URL ⟨http://www.sciencedirect.com/science/article/pii/S096980431730218X⟩.

Bergeson, S., Peatross, J., Ware, M., 2017a. Precision long-term measurements of beta-decay-rate ratios in a controlled environment. Phys. Lett. B 767, 171–176. https://doi.org/10.1016/j.physletb.2017.01.030.(URL ⟨http://www.sciencedirect.com/science/article/pii/S0370269317300485⟩).

Bergeson, S.D., Ware, M.J., Hawk, J., 2017b. On the Use of Nai Scintillation for High Stability Nuclear Decayrate Measurements. arXiv:arXiv:1707.03392.

Bevington, P., Robinson, D.K., 2003. Data Reduction and Error Analysis in the Physical Sciences, 3rd edition. McGraw-Hill Education, New York.

Borrello, J.A., Wuosmaa, A., Watts, M., 2018. Non-dependence of nuclear decay rates of ^{123}I and ^{99m}Tc on Earth-Sun distance. Appl. Radiat. Isot. 132, 189–194. https://doi.org/10.1016/j.apradiso.2017.12.006.(URL ⟨http://www.sciencedirect.com/science/article/pii/S0969804317311223⟩).

Chakraborty, B., Davies, C.T.H., DeTar, C., El-Khadra, A.X., Gámiz, E., Gottlieb, S., Hatton, D., Koponen, J., Kronfeld, A.S., Laiho, J., Lepage, G.P., Liu, Y., Mackenzie, P.B., McNeile, C., Neil, E.T., Simone, J.N., Sugar, R., Toussaint, D., Van de Water, R.S., Vaquero, A., 2018. Strong-isospin-breaking correction to the muon anomalous magnetic moment from lattice QCD at the physical point. Phys. Rev. Lett. 120, 152001. https://doi.org/10.1103/PhysRevLett.120.152001.

Cooper, P.S., 2009. Searching for modifications to the exponential radioactive decay law with the Cassini spacecraft. Astropart. Phys. 31 (4), 267–269. https://doi.org/10.1016/j.astropartphys.2009.02.005.(URL ⟨http://www.sciencedirect.com/science/article/pii/S0927650509000346⟩).

Desai, S., Liu, D.W., 2016. A search for evidence of solar rotation in Super-Kamiokande solar neutrino dataset. Astropart. Phys. 82, 86–92. https://doi.org/10.1016/j.astropartphys.2016.06.004.(URL ⟨http://www.sciencedirect.com/science/article/pii/S0927650516300834⟩).

Fischbach, E., Buncher, J.B., Gruenwald, J.T., Jenkins, J.H., Krause, D.E., Mattes, J.J., Newport, J.R., 2009. Time-dependent nuclear decay parameters: new evidence for new forces? Space Sci. Rev. 145 (3), 285–335. https://doi.org/10.1007/s11214-009-9518-5.

García-Bellido, J., Quirós, M., 1990. Extended inflation in scalar-tensor theories of gravity. Phys. Lett. B 243 (1), 45–51. https://doi.org/10.1016/0370-2693(90)90954-5.(URL ⟨http://www.sciencedirect.com/science/article/pii/0370269390909545⟩).

Jenkins, J.H., Herminghuysen, K.R., Blue, T.E., Fischbach, E., Javorsek II, D., Kauffman, A.C., Mundy, D.W., Sturrock, P.A., Talnagi, J.W., 2012. Additional experimental evidence for a solar influence on nuclear decay rates. Astropart. Phys. 37, 81–88. https://doi.org/10.1016/j.astropartphys.2012.07.008.(URL ⟨http://www.sciencedirect.com/science/article/pii/S0927650512001442⟩).

Kossert, K., Nähle, O.J., 2014. Long-term measurements of ^{36}Cl to investigate potential solar influence on the decay rate. Astropart. Phys. 55, 33–36. https://doi.org/10.1016/j.astropartphys.2014.02.001.(URL ⟨http://www.sciencedirect.com/science/article/pii/S0927650514000139⟩).

Kossert, K., Nähle, O.J., 2015. Disproof of solar influence on the decay rates of ^{90}Sr/^{90}Y. Astropart. Phys. 69, 18–23. https://doi.org/10.1016/j.astropartphys.2015.03.003.(URL ⟨http://www.sciencedirect.com/science/article/pii/S0927650515000432⟩).

Martins, C.J.A.P., 2017. The status of varying constants: a review of the physics, searches and implications. Rep. Prog. Phys. 80 (12), 126902(URL ⟨http://stacks.iop.org/0034-4885/80/i=12/a=126902⟩).

Meier, M.M., Wieler, R., 2014. No evidence for a decrease of nuclear decay rates with increasing heliocentric distance based on radiochronology of meteorites. Astropart. Phys. 55, 63–75. https://doi.org/10.1016/j.astropartphys.2014.01.004.(URL ⟨http://www.sciencedirect.com/science/article/pii/S0927650514000127⟩).

Nähle, O., Kossert, K., 2014. Comment on comparative study of beta-decay data for eight nuclides measured at the Physikalisch-Technische Bundesanstalt. Astropart. Phys. 59, 47–58. https://doi.org/10.1016/j.astropartphys.2014.11.005.(Astropart. Phys., 66, 2015, pp. 8–10. URL ⟨http://www.sciencedirect.com/science/article/pii/S0927650514001832⟩).

Norman, E.B., Browne, E., Shugart, H.A., Joshi, T.H., Firestone, R.B., 2009. Evidence against correlations between nuclear decay rates and EarthSun distance. Astropart. Phys. 31 (2), 135–137. https://doi.org/10.1016/j.astropartphys.2008.12.004.(URL ⟨http://www.sciencedirect.com/science/article/pii/S0927650508001928⟩).

Planck Collaboration, Ade, P.A.R., Aghanim, N., Armitage-Caplan, C., Arnaud, M., Ashdown, M., Atrio-Barandela, F., Aumont, J., Baccigalupi, C., Banday, A.J., Barreiro, R.B., Bartlett, J.G., Battaner, E., Benabed, K., Benoît, A., Benoit-Lévy, A., Bernard, J.P., Bersanelli, M., Bielewicz, P., Bobin, J., Bock, J.J., Bonaldi, A., Bond, J.R., Borrill, J., Bouchet, F.R., Bridges, M., Bucher, M., Burigana, C., Butler, R.C., Calabrese, E., Cappellini, B., Cardoso, J.F., Catalano, A., Challinor, A., Chamballu, A., Chary, R.R., Chen, X., Chiang, H.C., Chiang, L.Y., Christensen, P.R., Church, S., Clements, D.L., Colombi, S., Colombo, L.P.L., Couchot, F., Coulais, A., Crill, B.P., Curto, A., Cuttaia, F., Danese, L., Davies, R.D., Davis, R.J., de Bernardis, P., de Rosa, A., de Zotti, G., Delabrouille, J., Delouis, J.M., Désert, F.X., Dickinson, C., Diego, J.M., Dolag, K., Dole, H., Donzelli, S., Doré, O., Douspis, M., Dunkley, J., Dupac, X., Efstathiou, G., Elsner, F., Enßlin, T.A., Eriksen, H.K., Finelli, F., Forni, O., Chiang, M., Fraisse, A.A., Franceschi, E., Gaier, T.C., Galeotta, S., Galli, S., Ganga, K., Giard, M., Giardino, G., Giraud-Héraud, Y., Gjerløw, E., González-Nuevo, J., Górski, K.M., Gratton, S., Gregorio, A., Gruppuso, A., Gudmundsson, J.E., Haissinski, J., Hamann, J., Hansen, F.K., Hanson, D., Harrison, D., Henrot-Versillé, S., Hernández-Monteagudo, C., Herranz, D., Hildebrandt, S.R., Hivon, E., Hobson, M., Holmes, W.A., Hornstrup, A., Hou, Z., Hovest, W., Huffenberger, K.M., Jaffe, A.H., Jaffe, T.R., Jewell, J., Jones, W.C., Juvela, M., Keihänen, E., Keskitalo, R., Kisner, T.S., Kneissl, R., Knoche, J., Knox, L., Kunz, M., Kurki-Suonio, H., Lagache, G., Lähteenmäki, A., Lamarre, J.M., Lasenby, A., Lattanzi, M., Laureijs, R.J., Lawrence, C.R., Leach, S., Leahy, J.P., Leonardi, R., León-Tavares, J., Lesgourgues, J., Lewis, A., Liguori, M., Lilje, P.B., Linden-Vørnle, M., López-Caniego, M., Lubin, P.M., Macías-Pérez, J.F., Maffei, B., Maino, D., Mandolesi, N., Maris, M., Marshall, D.J., Martin, P.G., Martínez- González, E., Masi, S., Massardi, M., Matarrese, S., Matthai, F., Mazzotta, P., Meinhold, P.R., Melchiorri, A., Melin, J.B., Mendes, L., Menegoni, E., Mennella, A., Migliaccio, M., Millea, M., Mitra, S., Miville- Deschênes, M.A., Moneti, A., Montier, L., Morgante, G., Mortlock, D., Moss, A., Munshi, D., Murphy, J.A., Naselsky, P., Nati, F., Natoli, P., Netterfield, C.B., Nørgaard-Nielsen, H.U., Noviello, F., Novikov, D., Novikov, I., O'Dwyer, I.J., Osborne, S., Oxborrow, C.A., Paci, F., Pagano, L., Pajot, F., Paladini, R., Paoletti, D., Partridge, B., Pasian, F., Patanchon, G., Pearson, D., Patanchon, T.J., Peiris, H.V., Perdereau, O., Perotto, L., Perrotta, F., Pettorino, V., Piacentini, F., Piat, M., Pierpaoli, E., Pietrobon, D., Plaszczynski, S., Platania, P., Pointecouteau, E., Polenta, G., Ponthieu, N., Popa, L., Poutanen, T., Pratt, G.W., Prézeau, G., Prunet, S., Puget, J.L., Rachen, J.P., Reach, W.T., Rebolo, R., Reinecke, M., Remazeilles, M., Renault, C., Ricciardi, S., Riller, T., Ristorcelli, I., Rocha, G., Rosset, C., Roudier, G., Rowan-Robinson, M., Rubiño-Martín, J.A., Rusholme, B., Hobson, M., Santos, D., Savelainen, M., Savini, G., Scott, D., Seiffert, M.D., Shellard, E.P.S., Spencer, L.D., Starck, M., Stolyarov, V., Stompor, R., Sudiwala, R., Sunyaev, R., Sureau, F., Sutton, D., Suur-Uski, A.S., Sygnet, J.F., Spencer, J.A., Tavagnacco, D., Terenzi, L., Toffolatti, L., Tomasi, M., Tristram, M., Tucci, M., Tuovinen, J., Türler, M., Umana, G., Valenziano, L., Valiviita, J., Van Tent, B., Vielva, P., Villa, F., Vittorio, N., Wade, L.A., Wandelt, B.D., Wehus, I.K., White, M., White, S.D.M., Wilkinson, A., Yvon, D., Zacchei, A., Zonca, A., 2014. Planck 2013 results. XVI. Cosmological parameters. Astron. Astrophys. 571, A16. https://doi.org/10.1051/0004-6361/201321591.

Pommé, S., Stroh, H., Paepen, J., Ammel, R.V., Marouli, M., Altzitzoglou, T., Hult, M., Kossert, K., Nähle, O., Schrader, H., Juget, F., Bailat, C., Nedjadi, Y., Bochud, F., Buchillier, T., Michotte, C., Courte, S., van Rooy, M., van Staden, M., Lubbe, J., Simpson, B., Fazio, A., Felice, P.D., Jackson, T., Wyngaardt, W.V., Reinhard, M., Golya, J., Bourke, S., Roy, T., Galea, R., Keightley, J., Ferreira, K., Collins, S., Ceccatelli, A., Unterweger, M., Fitzgerald, R., Bergeron, D., Pibida, L., Verheyen, L., Bruggeman, M., Vodenik, B., Korun, M., Chisté, V., Amiot, M.-N., 2016. Evidence against solar influence on nuclear decay constants. Phys. Lett. B 761, 281–286. https://doi.org/10.1016/j.physletb.2016.08.038.(URL ⟨http://www.sciencedirect.com/science/article/pii/S0370269316304580⟩).

Pommé, S., Stroh, H., Paepen, J., Ammel, R.V., Marouli, M., Altzitzoglou, T., Hult, M., Kossert, K., Nähle, O., Schrader, H., Juget, F., Bailat, C., Nedjadi, Y., Bochud, F., Buchillier, T., Michotte, C., Courte, S., van Rooy, M.W., van Staden, M.J., Lubbe, J., Simpson, B.R.S., Fazio, A., Felice, P.D., Jackson, T.W., Wyngaardt, W.M.V., Reinhard, M.I., Golya, J., Bourke, S., Roy, T., Galea, R., Keightley, J.D., Ferreira, K.M., Collins, S.M., Ceccatelli, A., Verheyen, L., Bruggeman, M., Vodenik, B., Korun, M., Chisté, V., Amiot, M.-N., 2017a. On decay constants. Metrologia 54 (1), 1(URL ⟨http://stacks.iop.org/0026-1394/54/i=1/a=1⟩).

Pommé, S., Stroh, H., Paepen, J., Ammel, R.V., Marouli, M., Altzitzoglou, T., Hult, M., Kossert, K., Nähle, O., Schrader, H., Juget, F., Bailat, C., Nedjadi, Y., Bochud, F., Buchillier, T., Michotte, C., Courte, S., van Rooy, M.W., van Staden, M.J., Lubbe, J., Simpson, B.R.S., Fazio, A., Felice, P.D., Jackson, T.W., Wyngaardt, W.M.V., Reinhard, M.I., Golya, J., Bourke, S., Roy, T., Galea, R., Keightley, J.D., Ferreira, K.M., Collins, S.M., Ceccatelli, A., Verheyen, L., Bruggeman, M., Vodenik, B., Korun, M., Chisté, V., Amiot, M.-N., 2017b. On decay constants and orbital distance to the Sun – part II: beta minus decay. Metrologia 54 (1), 19(URL ⟨http://stacks.iop.org/0026-1394/54/i=1/a=19⟩).

Pommé, S., Stroh, H., Paepen, J., Ammel, R.V., Marouli, M., Altzitzoglou, T., Hult, M., Kossert, K., Nähle, O., Schrader, H., Juget, F., Bailat, C., Nedjadi, Y., Bochud, F., Buchillier, T., Michotte, C., Courte, S., van Rooy, M.W., van Staden, M.J., Lubbe, J., Simpson, B.R.S., Fazio, A., Felice, P.D., Jackson, T.W., Wyngaardt, W.M.V., Reinhard, M.I., Golya, J., Bourke, S., Roy, T., Galea, R., Keightley, J.D., Ferreira, K.M., Collins, S.M., Ceccatelli, A., Verheyen, L., Bruggeman, M., Vodenik, B., Korun, M., Chisté, V., Amiot, M.-N., 2017c. On decay constants and orbital distance to the Sun – part III: beta plus and electron capture decay. Metrologia 54 (1), 36(URL ⟨http://stacks.iop.org/0026-1394/54/i=1/a=36⟩).

Pommé, S., Kossert, K., Nähle, O., 2017d. On the claim of modulations in ^{36}Cl beta decay and their association with solar rotation. Sol. Phys. 292 (11), 162. https://doi.org/10.1007/s11207-017-1187-z.

Pommé, S., Stroh, H., Altzitzoglou, T., Paepen, J., Ammel, R.V., Kossert, K., Nhle, O., Keightley, J., Ferreira, K., Verheyen, L., Bruggeman, M., 2018a. Is decay constant? Applied radiation and isotopes. In: Proceedings of the 21st International Conference

on Radionuclide Metrology and its Applications. ICRM 2017, 134, pp. 6–12. ⟨https://dx.doi.org/10.1016/j.apradiso.2017.09.002⟩. URL ⟨http://www.sciencedirect.com/science/article/pii/S0969804317303822⟩.

Pommé, S., Lutter, G., Marouli, M., Kossert, K., Nähle, O., 2018b. On the claim of modulations in radon decay and their association with solar rotation. Astropart. Phys. 97, 38–45. https://doi.org/10.1016/j.astropartphys.2017.10.011.(URL ⟨http://www.sciencedirect.com/science/article/pii/S0927650517302323⟩).

Safronova, M.S., Budker, D., DeMille, D., Kimball, D.F.J., Derevianko, A., Clark, C.W., 2018. Search for new physics with atoms and molecules. Rev. Mod. Phys. 90, 025008. https://doi.org/10.1103/RevModPhys.90.025008.

Schrader, H., 2016. Seasonal variations of decay rate measurement data and their interpretation. Appl. Radiat. Isot. 114, 202–213. https://doi.org/10.1016/j.apradiso.2016.05.001.(URL ⟨http://www.sciencedirect.com/science/article/pii/S0969804316301610⟩).

Siegert, H., Schrader, H., Schötzig, U., 1998. Half-life measurements of europium radionuclides and the long-term stability of detectors. Appl. Radiat. Isot. 49 (911), 1397–1401. https://doi.org/10.1016/S0969-8043(97)10082-3.(URL ⟨http://www.sciencedirect.com/science/article/pii/S0969804397100823⟩).

Spergel, D.N., Verde, L., Peiris, H.V., Komatsu, E., Nolta, M.R., Bennett, C.L., Halpern, M., Hinshaw, G., Jarosik, N., Kogut, A., Limon, M., Meyer, S.S., Page, L., Tucker, G.S., Weiland, J.L., Wollack, E., Wright, E.L., 2003. First-year Wilkinson microwave anisotropy probe (WMAP) observations: determination of cosmological parameters. Astrophys. J. Suppl. Ser. 148 (1), 175(URL ⟨http://stacks.iop.org/0067-0049/148/i=1/a=175⟩).

Stancil, D.D., Yegen, S.B., Dickey, D.A., Gould, C.R., 2017. Search for possible solar influences in Ra-226 decays. Results Phys. 7, 385–406. https://doi.org/10.1016/j.rinp.2016.12.051.(URL ⟨http://www.sciencedirect.com/science/article/pii/S2211379716307987⟩).

Steinwachs, C.F., van der Wild, M.L., 2018. Quantum gravitational corrections from the Wheeler-DeWitt equation for scalar-tensor theories. Class. Quantum Gravity 35 (13), 135010(URL ⟨http://stacks.iop.org/0264-9381/35/i=13/a=135010⟩).

Sturrock, P., Bertello, L., Fischbach, E., Javorsek, D., Jenkins, J., Kosovichev, A., Parkhomov, A., 2013. An analysis of apparent r-mode oscillations in solar activity, the solar diameter, the solar neutrino flux, and nuclear decay rates, with implications concerning the Sun's internal structure and rotation, and neutrino processes. Astropart. Phys. 42, 62–69. https://doi.org/10.1016/j.astropartphys.2012.11.011.(URL ⟨http://www.sciencedirect.com/science/article/pii/S0927650512002150⟩).

Sturrock, P., Steinitz, G., Fischbach, E., 2018. Analysis of gamma radiation from a radon source. II: indications of influences of both solar and cosmic neutrinos on beta decays. Astropart. Phys. 100, 1–12. https://doi.org/10.1016/j.astropartphys.2018.02.003.(URL ⟨http://www.sciencedirect.com/science/article/pii/S0927650517302797⟩).

Towers, S., 2013. Improving the control of systematic uncertainties in precision measurements of radionuclide half-life. Appl. Radiat. Isot. 77, 110–114. https://doi.org/10.1016/j.apradiso.2013.03.003.(URL ⟨http://www.sciencedirect.com/science/article/pii/S0969804313000857⟩).

Udem, T., 2018. Quantum electrodynamics and the proton size. Nat. Phys. 14 (6). https://doi.org/10.1038/s41567-018-0166-0. 632–632.

Ware, M.J., Bergeson, S.D., Ellsworth, J.E., Groesbeck, M., Hansen, J.E., Pace, D., Peatross, J., 2015. Instrument for precision long-term β-decay rate measurements. Rev. Sci. Instrum. 86 (7). https://doi.org/10.1063/1.4926346.(URL ⟨http://scitation.aip.org/content/aip/journal/rsi/86/7/10.1063/1.4926346⟩).